DOI: 10.1111/mice.12929

RESEARCH ARTICLE

COMPUTER-AIDED CIVIL AND INFRASTRUCTURE ENGINEERING WILEY

Efficient estimation of tuned liquid column damper inerter (TLCDI) parameters for seismic control of base-isolated structures

Chiara Masnata[1] | **Alberto Di Matteo**[1] | **Christoph Adam**[2] | **Antonina Pirrotta**[1]

[1]Department of Engineering, University of Palermo, Palermo, Italy

[2]Unit of Applied Mechanics, University of Innsbruck, Innsbruck, Austria

Correspondence
Christoph Adam, Unit of Applied Mechanics, University of Innsbruck, Technikerstr. 13, Innsbruck, Austria
Email: christoph.adam@uibk.ac.at

Abstract

This paper presents an enhanced base-isolation (BI) system equipped with a novel passive control device composed of a tuned liquid damper and an inerter (TLCDI). With the aim of reducing the seismic response of BI systems, this contribution focuses on the design of the TLCDI providing analytical solutions for the optimal TLCDI parameters, easily implementable in the design phase. The effectiveness of the proposed approach in terms of seismic response reduction and computational gain is validated by comparison with classical numerical optimization techniques. The control performance of two different base-isolated TLCDI-controlled structures is assessed by employing real-ground motion records, and relevant comparisons with both uncontrolled base-isolated structures and equipped with a conventional TLCD are presented.

1 | INTRODUCTION

Seismic base isolation (BI) is undoubtedly one of the most efficient control strategies conceived to protect structures from damage due to earthquakes (Kelly, 1990). It belongs to the category of the so-called passive systems, which, unlike active systems, do not require an external power source and are therefore relatively inexpensive and always functional even in the event of a power failure. Its effectiveness relies on the decoupling effect of the structure from the ground motion provided by a laterally flexible layer placed in between the main structure (superstructure) and its foundation. This isolation effect leads to a longer fundamental natural period, compared to fixed-base structures, preventing in this way large deformations and high accelerations in the superstructure. Indeed, earthquake-induced vibrations occurring in the isolation subsystem are only partially transmitted to the superstructure, which mostly experiences a rigid translation behaving like a single block. However, these benefits come at the expense of large displacements of the BI subsystem that may be detrimental to the integrity of the employed isolation devices, namely, the isolators (Kelly, 1999). Therefore, to protect isolators from damage caused by excessive lateral displacements and to improve the performance of the conventional BI system, their combination with active or semi-active control devices led to the concept of hybrid or smart BI systems for improved resilience to multiple hazards and extreme events (Aldemir et al., 2012; Javadinasab Hormozabad et al., 2021).

Active systems require substantial power sources to generate control forces via actuators to allow the structure to adjust its response during earthquakes, while limited power, sometimes even a battery, is often sufficient for semi-active systems (Ghaedi et al., 2017). In this context, Gutierrez Soto and Adeli (2018) investigated active

and semi-active strategies to improve the dynamic performance of an eight-story L-shaped base-isolated structure to achieve a real-time vibration control. In particular, they demonstrated that the installation of actuators at the base and applying the concept of replicator dynamics can provide an additional dampening effect for the BI system (Gutierrez Soto & Adeli, 2018). The same authors also investigated the integration of semi-active magnetorheological dampers in base-isolated highway bridges and proved their beneficial effect on reducing the mid-span displacement of bridges under seismic actions (Gutierrez Soto & Adeli, 2019).

Other researchers also considered passive mechanical damping devices, such as the well-known tuned mass dampers (TMDs; Den Hartog, 1956), tuned liquid damper (TLDs; Banerji et al., 2000) and tuned liquid column dampers (TLCDs; Hochrainer & Ziegler, 2006) as a complement to improve BI systems. In this regard, Yang et al. (1991) have shown that the use of an oscillating secondary mass, such as the TMD, may be more effective and advantageous in reducing the response of tall, isolated buildings than the application of an active control system alone. Moreover, TMDs have thoroughly proved to be most effective at reducing the displacement demand of low-damped BI systems while preserving the small interstory drift, overall leading to better performance than increasing the damping of the isolators (Taniguchi et al., 2008; Tsai, 1995). However, compared to the more common TMDs, TLDs and TLCDs devices proved to be particularly convenient for BI systems (Adam et al., 2017; Love et al., 2011). TLDs are generally rectangular or cylinder-shaped devices, and their effectiveness relies on the interaction force between liquid and side walls and wave breaking to absorb vibration energy. On the other hand, TLCDs are designed as U-shaped tanks filled with liquid (commonly water) that dissipate energy through a combination of liquid motion, the restoring force due to gravity, and the damping force due to inherent head loss characteristics (Zhu et al., 2019). TLDs and TLCDs comprise several advantageous features, such as low cost, easy implementation, the possibility to directly tune their parameters by adjusting the quantity of liquid, the lack of required maintenance, and the possibility to use the liquid contained in the tank as a secondary emergency water source (Gutierrez Soto & Adeli, 2013). However, despite the well-known beneficial effects of TLDs and TLCDs for seismic response reduction in BI systems, these devices may require excessively large mass and large spaces to achieve higher efficiency (Kim & Adeli, 2005a).

Therefore, to face these issues, innovative types of liquid-based dampers have been explored in combination with other devices. The idea to retain the advantage of both the TMD and TLD to a certain extent, while partially eliminating the limitations of each, led to the alternative configurations of the hybrid mass liquid damper (Banerji & Samanta, 2011) and tuned liquid mass damper (Pandey et al., 2022) comprising a secondary mass attached to the primary structure through a spring-dashpot system and supporting a liquid damper. Similarly, a combination of a TLCD with TMD, referred to as a combined tuned damper, was investigated by L. Wang et al. (2016) and its efficacy experimentally validated by Di Matteo et al. (2017). In order to increase the effectiveness of these passive control devices while maintaining the advantage of not requiring an external power supply, their combination with mass amplification mechanisms has been explored, making them more competitive with active/semi-active systems. In this regard, the first integration of inerter-based devices into the traditional TMD has been considered to form the so-called TMD inerter (TMDI; Marian & Giaralis, 2014). Specifically, the inerter (Smith, 2002) is a two-terminal mechanical device that generates a resisting force proportional to the accelerations of its extremities, with a constant referred to as inertance, measured in mass units. There are still only a few studies on tested inerter devices and real engineering applications. Most real inerter devices, characterized by an inertance hundreds of times larger than their physical mass, have been manufactured by exploiting the rotational inertia of mechanisms with gears, flywheels, and fluid flow (Smith, 2020). The incorporation of inerter into different types of TMDs has proven to be particularly advantageous to realize more powerful devices without extra weight (Di Matteo et al., 2019; Masnata et al., 2020). In view of the above, and considering that TLCDs can achieve the same motion reduction level as traditional TMDs with significant practical advantages, if properly designed (Xu et al., 1992), the inerter has been also integrated into the classical TLCD to constitute a device known in the literature as TLCD inerter (TLCDI; Wang et al., 2020a). Notably, the inerter in the introduced TLCDI configuration provides a mass amplification effect of the system to which it is connected (Marian & Giaralis, 2014; Takewaki et al., 2012), making the TLCDI behave like a TLCD with a larger mass, to achieve enhanced performance, compared to the classical TLCD (Wang et al., 2020a). Unlike the classical TLCD, the TLCDI is mounted on a roller support and connected to the base slab via a spring-damper system and to the ground via an inerter. Therefore, in this case, the energy dissipation effect of the TLCDI is due to the horizontal motion of the device itself and of the liquid inside a U-tube container.

In this context, it has been shown in Wang et al. (2020a) that by employing a TLCDI to reduce the displacement of fixed-base structures during severe earthquakes, a significant improvement can be achieved over the classical TLCD. In addition, an unconventional seismic protection

strategy employing the TLCDI as a link between adjacent high-rise buildings has also demonstrated the effectiveness of this device in mitigating the acceleration responses (Wang et al., 2020b).

Clearly, the optimal design of the TLCDI plays a pivotal role in obtaining the best control performance. It should be noted, however, that in all the previous studies, many of the optimal TLCDI parameters were simultaneously derived for TLCDI-controlled structures by means of complex numerical procedures based on the minimization of different objective functions such as the peak displacement and absolute acceleration responses (Wang et al., 2020a). Therefore, these multi-objective optimization procedures may be computationally demanding in a design phase (H. S. Kim & Roschke, 2006), even leading in some cases to unrealistic parameters not applicable in real design processes (Wang et al., 2020a). To face this issue, an optimal design of the TLCDI through direct closed form solutions and ready-to-use design charts has been recently proposed in Di Matteo et al. (2022).

Although the use of conventional TLCDs has been considered a promising strategy for controlling base-isolated structures (Di Matteo et al., 2018; Furtmüller et al., 2019), to the best of the authors' knowledge, there are currently no studies in the literature on the use of TLCDI for base-isolated structures.

On this basis, in this study, a BI system endowed with a TLCDI device is considered, and the enhanced control performances of this novel device are highlighted. Specifically, as a first novel contribution, the present work focuses on providing analytical closed-form solutions for determining, in a straightforward way and without resorting to unwieldy numerical algorithms, the TLCDI optimal design parameters for a seismically excited multi-degree-of-freedom (MDOF) base-isolated structure. In this regard, the nonlinear equations of motion are established, and TLCDI optimal parameters are evaluated by taking into account a statistical linearization technique (SLT). Specifically, the proposed optimization procedure is based on the minimization of the BI subsystem displacement variance, which is found in a closed form on the base of some reasonable assumptions. In particular, a Gaussian white noise has been considered as base excitation and a linear undamped single-degree-of-freedom (SDOF) system has been used to model the base-isolated structure. Most importantly, these closed-form expressions yield very accurate results, without the need for computational effort as in classical numerical methods. It should be emphasized that the optimal parameters found in this work are rather different from the TLCDI optimal parameters recently presented by Wang et al. (2020a), and a direct comparison is not possible for several reasons. First, the optimization procedure proposed in the present study was formulated with the specific purpose of reducing the base displacement of BI systems, whereas the study conducted by Wang et al. (2020a) focused on fixed-base SDOF structures. Second, unlike the proposed optimization, the TLCDI parameters found by Wang et al. (2020a) are the result of numerical multi-objective minimization and no closed forms of these parameters were obtained.

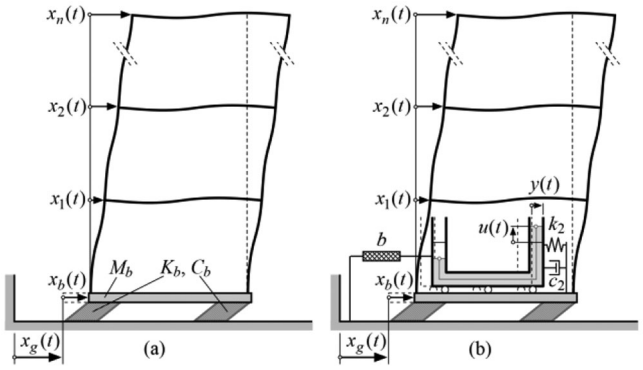

FIGURE 1 (a) MDOF base-isolated structure; (b) MDOF base-isolated tuned liquid column damper inerter (TLCDI)-controlled structure

The accuracy of the proposed approximate closed-form formula is investigated by comparison with a more elaborate and unwieldy numerical procedure performed on the original damped MDOF base-isolated structure. In addition, a thorough seismic analysis is performed in which a five-story base-isolated structure and a 20-story base-isolated structure equipped with TLCDI are subjected to a set of 44 recorded accelerograms as base excitation, varying in magnitude and soil site type. In this regard, the effectiveness of the TLCDI device is assessed by comparisons with the pertinent responses of the BI system alone or endowed with the classical TLCD device.

2 | PROBLEM FORMULATION

Consider a base-isolated MDOF structure with the superstructure having n degrees of freedom as shown in Figure 1a and subjected to a horizontal ground acceleration $\ddot{x}_g(t)$. The $n \times n$ mass, damping, and stiffness matrix of the main structure are denoted as $\mathbf{M}_s$, $\mathbf{C}_s$, and $\mathbf{K}_s$, respectively, the $n \times 1$ vector $\boldsymbol{x}_s(t)$ contains the nodal displacements of the superstructure with respect to the base.

The BI subsystem with mass m_b, stiffness K_b, and damping parameter C_b is assumed to be linear, and its displacement relative to the ground is denoted as $x_b(t)$. Then, the $n + 1$ equations of motion of the superstructure coupled with the BI subsystem become (Kelly, 1997)

$$\begin{bmatrix} \mathbf{M}_s & \mathbf{M}_s\mathbf{r} \\ \mathbf{r}^{\mathrm{T}}\mathbf{M}_s & M_{tot} \end{bmatrix} \begin{bmatrix} \ddot{\boldsymbol{x}}_s(t) \\ \ddot{x}_b(t) \end{bmatrix} + \begin{bmatrix} \mathbf{C}_s & \mathbf{0} \\ \mathbf{0} & C_b \end{bmatrix} \begin{bmatrix} \dot{\boldsymbol{x}}_s(t) \\ \dot{x}_b(t) \end{bmatrix} + \begin{bmatrix} \mathbf{K}_s & \mathbf{0} \\ \mathbf{0} & K_b \end{bmatrix} \begin{bmatrix} \boldsymbol{x}_s(t) \\ x_b(t) \end{bmatrix} = -\begin{bmatrix} \mathbf{M}_s\mathbf{r} \\ M_{tot} \end{bmatrix} \ddot{x}_g(t) \tag{1}$$

where the total system mass is composed of the mass of the BI subsystem and the total mass of the superstructure: $M_{tot} = m_b + \mathbf{r}^{\mathrm{T}}\mathbf{M}_s\mathbf{r}$ with $\mathbf{r} = [1, \dots, 1]^{\mathrm{T}}$ representing the $n \times 1$ quasi-static influence vector, and the apex T denotes the transpose operation. Bold lowercase characters indicate vectors and uppercase matrices and not bolded italic characters stand for scalars and constants. A dot over a variable indicates the derivation with respect to time t.

To reduce the base displacements, the base-isolated structure is equipped with a TLCDI device attached to the base of the isolated structure as shown in Figure 1b.

The TLCDI device depicted in Figure 2 consists of a U-shape tube with dimensions L_v and L_h for the vertical and horizontal liquid length, respectively. Thus, $L = L_h + 2L_v$ is the total length of the liquid in the container.

The liquid tank is characterized by the cross-sectional area A and its mass is M_c, while the liquid mass is $m_l = \rho AL$ being ρ the density of the liquid. The TLCDI is connected to the BI subsystem by a spring and a damper with stiffness and damping coefficient k_2 and c_2, respectively, and to the ground by an inerter element with inertance b. The vertical motion of the liquid in the U-shape tube is denoted as $u(t)$, while the horizontal motion of the container relative to the base is $y(t)$.

The response of this TLCDI-equipped MDOF base-isolated structure subjected to a horizontal ground acceleration is governed by the following set of $n + 3$ nonlinear differential equations:

$$\begin{bmatrix} \mathbf{M}_s & \mathbf{M}_s\mathbf{r} & \mathbf{0} & \mathbf{0} \\ \mathbf{r}^{\mathrm{T}}\mathbf{M}_s & M_{tot} + \rho AL + M_c + b & \rho AL + M_c + b & \rho AL_h \\ \mathbf{0} & \rho AL + M_c + b & \rho AL + M_c + b & \rho AL_h \\ \mathbf{0} & \rho AL_h & \rho AL_h & \rho AL \end{bmatrix} \begin{bmatrix} \ddot{\boldsymbol{x}}_s(t) \\ \ddot{x}_b(t) \\ \ddot{y}(t) \\ \ddot{u}(t) \end{bmatrix} +$$

$$\begin{bmatrix} \boldsymbol{C}_s & \mathbf{0} & \mathbf{0} & \mathbf{0} \\ \mathbf{0} & C_b & 0 & 0 \\ \mathbf{0} & 0 & c_2 & 0 \\ \mathbf{0} & 0 & 0 & \frac{\rho A}{2}\xi\,|\dot{u}(t)| \end{bmatrix} \begin{bmatrix} \dot{\boldsymbol{x}}_s(t) \\ \dot{x}_b(t) \\ \dot{y}(t) \\ \dot{u}(t) \end{bmatrix} +$$

$$\begin{bmatrix} \boldsymbol{K}_s & \mathbf{0} & \mathbf{0} & \mathbf{0} \\ \mathbf{0} & K_b & 0 & 0 \\ \mathbf{0} & 0 & k_2 & 0 \\ \mathbf{0} & 0 & 0 & 2\rho Ag \end{bmatrix} \begin{bmatrix} \boldsymbol{x}_s(t) \\ x_b(t) \\ y(t) \\ u(t) \end{bmatrix} = -\begin{bmatrix} \mathbf{M}_s\mathbf{r} \\ M_{tot} + \rho AL + M_c \\ \rho AL + M_c \\ \rho AL_h \end{bmatrix} \ddot{x}_g(t) \tag{2}$$

where g is the gravity acceleration and ξ is the so-called head loss coefficient, introduced to represent the nonlinear effect governing the hydrodynamic head losses that arise during the motion of the liquid inside the vessel (Hitchcock et al., 1997; Wu et al., 2005). The nonlinear damping force $\rho A\xi|\dot{u}(t)|\dot{u}(t)/2$ in Equation (2) models the head losses resulting from the orifices inside the TLCDI and viscous interaction between the liquid and the container wall (Di Matteo et al., 2014, 2015, 2018). To achieve better control performance, this parameter can be adjusted by varying the width of the orifices inside the container as is common in semi-active control strategy (Kim & Adeli, 2005b). However, as customary for passive liquid-based absorbers, the value of ξ is assumed to be constant in this study.

Since the entire system behaves nonlinearly, minimizing the displacement demand of the isolation level may encounter computational difficulties in the optimal design of the TLCDI. For this reason, an equivalent linearization procedure, which facilitates the optimal design process, is considered.

2.1 | SLT

The nonlinear Equation (2) can be linearized by adopting procedures such as the SLT (Navarra et al., 2020; Roberts & Spanos, 1990). In this context, the BI system equipped with the TLCDI is assumed to be excited by a white Gaussian noise process with zero mean; hence, the responses are also stochastic processes, and they are indicated with capital letters as is common in the literature (Di Matteo et al., 2018). Specifically, the nonlinear elements in each equation can be linearized individually (Roberts & Spanos, 1990). Consequently, the original nonlinear system in Equation (2) can be replaced by a linear equivalent system by making full use of the powerful tool of SLT.

$$\begin{bmatrix} \mathbf{M}_s & \mathbf{M}_s\mathbf{r} & \mathbf{0} & \mathbf{0} \\ \mathbf{r}^{\mathrm{T}}\mathbf{M}_s/M_{tot} & 1+\mu_t+\beta & \mu_t+\beta & \alpha\mu_l \\ \mathbf{0} & 1 & 1 & \frac{\alpha\mu_l}{\mu_t+\beta} \\ \mathbf{0} & \alpha & \alpha & 1 \end{bmatrix} \begin{bmatrix} \ddot{\boldsymbol{X}}_s(t) \\ \ddot{X}_b(t) \\ \ddot{Y}(t) \\ \ddot{U}(t) \end{bmatrix} +$$

$$\begin{bmatrix} \boldsymbol{C}_s & \mathbf{0} & \mathbf{0} & \mathbf{0} \\ \mathbf{0} & 2\zeta_b\omega_b & 0 & 0 \\ \mathbf{0} & 0 & 2\zeta_2\omega_2 & 0 \\ \mathbf{0} & 0 & 0 & 2\zeta_l\omega_l \end{bmatrix} \begin{bmatrix} \dot{\boldsymbol{X}}_s(t) \\ \dot{X}_b(t) \\ \dot{Y}(t) \\ \dot{U}(t) \end{bmatrix} + \tag{3}$$

$$\begin{bmatrix} \boldsymbol{K}_s & \mathbf{0} & \mathbf{0} & \mathbf{0} \\ \mathbf{0} & \omega_b^2 & 0 & 0 \\ \mathbf{0} & 0 & \omega_2^2 & 0 \\ \mathbf{0} & 0 & 0 & \omega_l^2 \end{bmatrix} \begin{bmatrix} \boldsymbol{X}_s(t) \\ X_b(t) \\ Y(t) \\ U(t) \end{bmatrix} = -\begin{bmatrix} \mathbf{M}_s\mathbf{r} \\ 1+\mu_t \\ \frac{\mu_t}{\mu_t+\beta} \\ \alpha \end{bmatrix} \ddot{X}_g(t)$$

where the following terms have been introduced: $\omega_b = \sqrt{K_b/M_{tot}}$ and $\zeta_b = C_b/(2\omega_b M_{tot})$ are the natural frequency and damping ratio of the BI subsystem, respectively. Furthermore, $\alpha = L_h/L$ is the length ratio and $\beta = b/M_{tot}$ the inertance ratio while $\mu_t = \mu_l + \delta$ denotes the total mass ratio of the TLCDI where $\mu_l = \rho AL/M_{tot}$ and $\delta = M_c/M_{tot}$ are the liquid and the container mass ratio, respectively. In addition, $\omega_2 = \sqrt{k_2/(\rho AL + M_c + b)}$

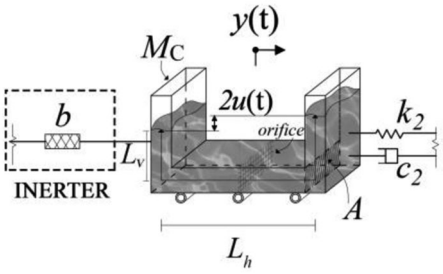

FIGURE 2 TLCDI device

is the natural frequency of the liquid container, $\zeta_2 = c_2/[2\omega_2(\rho AL + M_c + b)]$ is the damping ratio, and $\omega_l = \sqrt{2g/L}$ is the natural frequency of the liquid inside the TLCDI. The result is four coupled linear differential equations in which only the nonlinear expression $\rho A\xi|\dot{U}(t)|\dot{U}(t)/2$ in Equation (2), divided by ρAL, has been replaced by the equivalent linear damping force $2\zeta_l\omega_l\dot{U}(t)$. The variable ζ_l is an equivalent damping ratio.

The equivalent damping ratio ζ_l can be obtained by minimizing the mean square error between the nonlinear term and its equivalent linear one, which results in (Di Matteo et al., 2018):

$$\zeta_l = \frac{\xi}{2L\,\omega_l}\sqrt{\frac{2}{\pi}}\sigma_{\dot{U}} \tag{4}$$

In this relation, $\sigma_{\dot{U}}$ represents the standard deviation of the velocity of the liquid inside the TLCDI (compare with Appendix A). It should be noted that the estimation of ζ_l for design purposes is not trivial since $\sigma_{\dot{U}}$ is still unknown and depends inherently on ζ_l itself (Di Matteo et al., 2018). Thus, due to this dependence generally, an iterative solution procedure is required for determining ζ_l. In this procedure, the standard deviation of the liquid velocity $\sigma_{\dot{U}}$ with an arbitrary value initialization of ζ_l should be calculated first. Then, by substituting the obtained $\sigma_{\dot{U}}$ into Equation (4), a new value of ζ_l can be evaluated. This process is repeated until convergence is achieved between successive iterations. However, this iterative approach would require the use of complex numerical algorithms to determine the optimal parameters of the TLCDI. Thus, when practical analytical formulas for the optimal design parameters are sought, some simplified hypotheses should be reasonably introduced as described in the next section.

3 | OPTIMIZATION PROCEDURE

Now that the mathematical model of the BI system with TLCDI has been established, the focus is on the optimal design of the TLCDI. From Equation (3), the TLCDI parameters that affect the dynamic behavior of the system are the mass ratios μ_l and δ; the natural frequency ω_l and the equivalent damping ratio ζ_l of the liquid; the length ratio α; the natural frequency ω_2 and the damping ratio ζ_2 of the TLCDI container; and the inertance ratio β. It is obvious that the best control performance can only be achieved by an appropriate choice of the above parameters. Some of these variables, however, are often fixed a priori due to structural constraints as μ_l, β, δ, and α. Consequently, only the design parameters ζ_2, ζ_l, ω_l, and ω_2 (or equivalently the so-called frequency ratios $\nu_l = \omega_l/\omega_b$ and $\nu_2 = \omega_2/\omega_b$) must be chosen appropriately by an optimization technique.

As usually done in the relevant literature for TLCDI-based control strategies, these parameters can be sought by minimizing a specific quantity representative of the dynamic response of the structural system such as the response in terms of displacement or acceleration variance of the considered system as well as via an energy-based performance criterion (De Domenico & Ricciardi, 2018a; Zelleke & Matsagar, 2010). In this particular case, it is assumed that the target function of the optimization is the variance in terms of base displacement of the base-isolated structure. Specifically, the response variance in terms of base displacement can be expressed as

$$\sigma^2_{X_b} = G_0 \int_0^\infty |H_{X_b}(\omega)|^2\, d\omega \tag{5}$$

in which G_0 is the one-sided power spectral density (PSD) of the white noise input, and $H_{X_b}(\omega)$ is the BI subsystem displacement transfer function of the structure equipped with the TLCDI, defined as in Appendix A. Due to the complexity of the function $H_{X_b}(\omega)$, the variance in Equation (5) should be evaluated numerically, relying on cumbersome and time-consuming algorithms (Wang et al., 2020a; Zhao et al., 2019).

In addition, as described in the previous Section 2.1, an iterative procedure should be pursued to optimize the equivalent damping ratio ζ_l (Roberts & Spanos, 1990; Di Matteo et al., 2018). Therefore, in order to provide a tool to promptly compute the optimal TLCDI parameters in design phases, a direct analytical approach is proposed in the following.

3.1 | Approximate evaluation of the response variance

In order to determine the optimal design parameters of the TLCDI in a straightforward manner, a closed-form solution in terms of steady-state response statistics is proposed on

the base of simplifying assumptions. The first approximation concerns the response of the superstructure. Indeed, in the treatment of base isolation systems, it is common to approximate the superstructure as if it were a rigid block since the main displacement contribution comes from the isolation layer itself, which can undergo orders of magnitude larger displacements than those of the main structure. Therefore, the proposed optimization procedure can be applied considering an equivalent SDOF system characterized by a mass equal to the total mass of the original structure, as well as stiffness and damping of the isolation system (Figure 3).

In this manner, the original system of equations is significantly reduced to the following:

$$\tilde{\mathbf{M}}\ddot{\mathbf{Z}}(t)+\tilde{\mathbf{C}}\dot{\mathbf{Z}}(t)+\tilde{\mathbf{K}}\mathbf{Z}(t)=-\tilde{\mathbf{L}}\ddot{X}_g(t) \tag{6}$$

where $\mathbf{Z}(t)=[X_b(t)\ Y(t)\ U(t)]^T$ is the vector collecting the displacement of the degrees of freedom, $\tilde{\mathbf{L}}=[1+\mu_t\ \mu_t/(\mu_t+\beta)\ \alpha]^T$ is the location vector. The mass matrix $\tilde{\mathbf{M}}$, the damping matrix $\tilde{\mathbf{C}}$, and the stiffness matrix $\tilde{\mathbf{K}}$ are given as follows:

$$\begin{aligned}\tilde{\mathbf{M}}&=\begin{bmatrix}1+\mu_t+\beta & \mu_t+\beta & \alpha\mu_l\\ 1 & 1 & \alpha\mu_l/(\mu_t+\beta)\\ \alpha & \alpha & 1\end{bmatrix};\\ \tilde{\mathbf{C}}&=\begin{bmatrix}2\zeta_b\omega_b & 0 & 0\\ 0 & 2\zeta_2\omega_2 & 0\\ 0 & 0 & 2\zeta_l\omega_l\end{bmatrix};\ \tilde{\mathbf{K}}=\begin{bmatrix}\omega_b^2 & 0 & 0\\ 0 & \omega_2^2 & 0\\ 0 & 0 & \omega_l^2\end{bmatrix}\end{aligned} \tag{7}$$

The input is modeled as a zero-mean stationary Gaussian white noise process. Therefore, the corresponding Lyapunov equation for the evolution of the covariance matrix can be written as (Di Matteo et al., 2018)

$$\dot{\mathbf{\Sigma}}_{\mathbf{Q}}(t)=\mathbf{D}_{\mathbf{S}}\mathbf{\Sigma}_{\mathbf{Q}}(t)+\mathbf{\Sigma}_{\mathbf{Q}}(t)\mathbf{D}_{\mathbf{S}}^{\mathbf{T}}+\mathbf{G}_{\mathbf{S}}\mathbf{G}_{\mathbf{S}}^{\mathbf{T}}\pi G_0 \tag{8}$$

where $\mathbf{Q}=[\mathbf{Z}\ \dot{\mathbf{Z}}]^T$ is the vector of the state variables, $\mathbf{\Sigma}_{\mathbf{Q}}(t)$ denotes the covariance matrix given as

$$\mathbf{\Sigma}_{\mathbf{Q}}(t)=\begin{bmatrix}\sigma^2_{X_b} & \sigma^2_{X_bY} & \sigma^2_{X_bU} & \sigma^2_{X_b\dot{X}_b} & \sigma^2_{X_b\dot{Y}} & \sigma^2_{X_b\dot{U}}\\ & \sigma^2_{Y} & \sigma^2_{YU} & \sigma^2_{Y\dot{X}_b} & \sigma^2_{Y\dot{Y}} & \sigma^2_{Y\dot{U}}\\ & & \sigma^2_{U} & \sigma^2_{U\dot{X}_b} & \sigma^2_{U\dot{Y}} & \sigma^2_{U\dot{U}}\\ & & & \sigma^2_{\dot{X}_b} & \sigma^2_{\dot{X}_b\dot{Y}} & \sigma^2_{\dot{X}_b\dot{U}}\\ & sym & & & \sigma^2_{\dot{Y}} & \sigma^2_{\dot{Y}\dot{U}}\\ & & & & & \sigma^2_{\dot{U}}\end{bmatrix} \tag{9}$$

while $\mathbf{D}_{\mathbf{S}}$ and $\mathbf{G}_{\mathbf{S}}$ are given as

$$\mathbf{D}_{\mathbf{S}}=\begin{bmatrix}\mathbf{0} & \mathbf{I}_3\\ -\tilde{\mathbf{M}}^{-1}\tilde{\mathbf{K}} & -\tilde{\mathbf{M}}^{-1}\tilde{\mathbf{C}}\end{bmatrix};\ \mathbf{G}_{\mathbf{S}}=\begin{bmatrix}\mathbf{0}\\ -\tilde{\mathbf{L}}\end{bmatrix} \tag{10}$$

with $\mathbf{I}_3$ a 3×3 identity matrix.

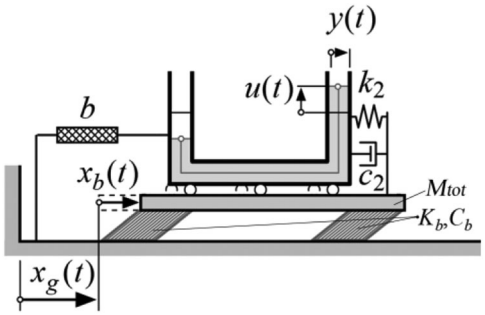

FIGURE 3 Simplified SDOF model equipped with TLCDI

In the case of stationarity, Equation (8) can be equated to zero to obtain the evolution of all the response statistics of the system in Equation (6). In order to find analytical expressions for the optimal TLCDI parameters, a closed form of $\sigma^2_{X_b}$ is additionally required by introducing further approximations.

Specifically, first, the approximate behavior of an undamped BI system can be sought as customary in many optimization procedures for passive vibration control systems (Di Matteo et al., 2019; Masnata et al., 2021). Moreover, the assumption that the liquid has no damping effect seems reasonable at this phase (Zhao et al., 2019) since the values of ζ_l are generally so small as to be negligible (Tait, 2008). Nevertheless, an estimate of ζ_l depending on the optimal design parameters determined below is given in the next section. Overall, on this base, only the design parameters ζ_2, ν_l, and ν_2 are sought, and introducing the aforementioned assumptions into Equation (8), after some algebra, the base displacement steady-state variance is derived in an analytical form as (Crandall & Mark, 1963)

$$\sigma^2_{X_b}=\phi_{X_b}\frac{\pi G_0}{4\omega_b^3} \tag{11}$$

in which $\phi_{X_b}=N/D$ with

$$\begin{aligned}N=&\alpha^6\mu_l^3(\beta+\mu_t)^2\nu_2^4+\nu_l^2(\beta+\mu_t)^2\left[1+(1+\mu_t)\left((1+\right.\right.\\&+\mu_t)\left(\mu_t-2+4\zeta_2^2(1+\mu_t)\right)+\beta\left(\mu_t-1+4\zeta_2^2(1+\right.\\&\left.\left.+\mu_t)\right)\right)\nu_2^2+(1+\mu_t)^2(1+\beta+\mu_t)^2\nu_2^4\Big)\Big](\nu_l^2-1)^2+\\&+\alpha^4\mu_l^2\Big[-2\nu_2^4(\beta+\mu_t)^3+\left(1-(\beta+\mu_t)\left(3-12\beta\zeta_2^2+\right.\right.\\&\left.+4\beta^2\zeta_2^2-\mu_t\left(\mu_t+4\zeta_2^2(3+\mu_t)\right)\right)\nu_2^2+(\beta+\mu_t)^2(6+\\&\left.+6\mu_t+\mu_t^2)\nu_2^4\right)\nu_l^2\Big]+\alpha^2\mu_l(\beta+\mu_t)\Big[(\beta+\mu_t)^3\nu_2^4+\\&-2(1+(-1-2\beta-2\beta(\beta-3)(1+\beta)\zeta_2^2-3\mu_t+\\&-2\left(\beta^2-3-8\beta\right)\zeta_2^2\mu_t+\left(\beta+(12+4\beta)\zeta_2^2\right)\mu_t^2+\\&+\left(1+4\zeta_2^2\right)\mu_t^3)\nu_2^2+(1+\mu_t)(\beta+\mu_t)(2+\beta(3+\mu_t)+\\&+4\mu_t+\mu_t^2)\nu_2^4)\nu_l^2+\left(2+2\left(-1+\mu_t\left(-3+\mu_t^2\right.\right.\right.\\&\left.\left.\left.+4\zeta_2^2(1+\mu_t)(2+\mu_t)\right)+\beta\left(\mu_t^2-2+4\zeta_2^2(1+\right.\right.\\&\left.\left.+\mu_t)(2+\mu_t)\right)\right)\nu_2^2+(1+\mu_t)(\beta+\mu_t)(4\beta+\\&\left.+2\mu_t\beta+(1+\mu_t)(5+2\mu_t))\nu_2^4\right)\nu_l^4\Big]\\D=&\nu_2\zeta_2\nu_l^2(\beta+\mu_t)\left[\beta-\alpha^2\mu_l+\mu_t-(\beta+\mu_t)\nu_l^2\right]^2\end{aligned} \tag{12}$$

Taking into account Equation (11), one may directly look for the minimum of the function $\phi_{X_b} = \phi_{X_b}(\zeta_2, \nu_l, \nu_2)$, which is independent of G_0 and of the natural frequency of the BI system ω_b.

In general, an analytical expression for the minimum of $\phi_{X_b}(\zeta_2, \nu_l, \nu_2)$ could be obtained by solving the nonlinear system of algebraic equations:

$$\frac{\partial \phi_{X_b}(\zeta_2, \nu_l, \nu_2)}{\partial \zeta_2} = 0 \tag{13a}$$

$$\frac{\partial \phi_{X_b}(\zeta_2, \nu_l, \nu_2)}{\partial \nu_2} = 0 \tag{13b}$$

$$\frac{\partial \phi_{X_b}(\zeta_2, \nu_l, \nu_2)}{\partial \nu_l} = 0 \tag{13c}$$

However, this procedure is often unfeasible, and thus the minimum of $\phi_{X_b}(\zeta_2, \nu_l, \nu_2)$ can be more easily found through numerical minimization procedures, such as those already implemented in many software packages (for instance FindMinimum in Mathematica or fminsearch in MATLAB environment). In this way, Equation (13) provides the optimal design parameter values ζ_2, ν_l and ν_2.

3.2 | Analytical expression of the optimal design parameters

Aiming at further reducing the computational complexity in a design phase of the TLCDI, an analytical expression of the optimal design parameters can be achieved considering some additional assumptions. As it can be seen in Equations (11) and (12), the function $\sigma^2_{X_b}$ depends on the mass ratios μ_l and μ_t. Since generally $\mu_l < 5\%$ and $\mu_t < 1\%$, solutions of Equation (13) can be approximated by assuming that the third and higher powers of μ_l, μ_t and their products can be neglected (Di Matteo et al., 2022).

In particular, under these assumptions, Equations (13a) and (13b) $\tilde{\nu}_{2,opt}(\nu_l)$ and $\tilde{\zeta}_{2,opt}(\nu_l)$ can be expressed as functions of ν_l as

$$\tilde{\nu}_{2,opt}(\nu_l) = \sqrt{A/B} \tag{14a}$$

$$\tilde{\zeta}_{2,opt}(\nu_l) = \sqrt{C/D} \tag{14b}$$

with

$$A = 3\alpha^4\mu_l^2\nu_l^2 + 2\alpha^2\mu_l\nu_l^2(1 + 2\beta + 3\mu_t)\left(\nu_l^2 - 1\right) - \nu_l^2 \left[-\beta^2 - 2\beta + \mu_t\left(\beta^2\mu_t - 2 - 4\beta - 3\mu_t\right)\right]\left(\nu_l^2 - 1\right)^2 \tag{15a}$$

$$B = -4\alpha^4\mu_l^2\beta\left(\beta - 3\nu_l^2\right) + 2\left[\beta(1+\beta)^2 + (1+\beta)\left(1 + 5\beta + 2\beta^2\right)\mu_t + (4 + \beta(2+\beta)(6+\beta))\mu_t^2\right]\nu_l^2\left(\nu_l^2 - 1\right)^2 + +2\alpha^2\mu_l\left[\beta^3 + 3\mu_t\beta^2 - 2\nu_l^2\left(2\beta + 3\beta^2 + (2+\beta)(1+4\beta)\mu_t\right) + \nu_l^4\left(5\beta + 4\beta^2 + \left(5 + 16\beta + 6\beta^2\right)\mu_t\right)\right] \tag{15b}$$

$$C = -\nu_l^2\left[4\beta^2 + 3\beta^3 + \left(8\beta + 21\beta^2 + 8\beta^3\right)\mu_t + \left(4 + 3\beta\left(11 + 12\beta + 2\beta^2\right)\right)\mu_t^2\right]\left(\nu_l^2 - 1\right)^3 + \alpha^4\mu_l^2\left[(4+\beta)(1+8\beta)\nu_l^2 - 12\beta^2 - \nu_l^4(8 + 25\beta)\right] + - \alpha^2\mu_l\left(\nu_l^2 - 1\right)\left[4\beta^3 + 12\beta^2\mu_t - \nu_l^2\left(8\beta + 21\beta^2 + \left(8 + 66\beta + 40\beta^2\right)\mu_t\right) + \nu_l^4\left(12\beta + 13\beta^2 + 2\mu_t\left(6 + 29\beta + 16\beta^2\right)\right)\right] \tag{15c}$$

$$D = -8\nu_l^2\left(\nu_l^2 - 1\right)^3\left[\beta(1+\beta)(2+\beta) + \mu_t\left(2 + \beta(4+\beta)(3+2\beta) + \left(9 + 25\beta + 12\beta^2\right)\mu_t\right)\right] - 8\nu_l^2\alpha^4\mu_l^2\beta\left[(\beta - 3)(5 + 4\beta) + \nu_l^2\left(18 + \beta - \beta^2\right)\right] + - 8\nu_l^2\alpha^2\mu_l\left(\nu_l^2 - 1\right)\left[\beta\left(\beta^3 - 9 - 10\beta + \nu_l^2(11 + 7\beta)\right) + \mu_t\left(-9 + 2\beta\left(2\beta^2 - 20 - 9\beta\right) + \nu_l^2\left(11 + 40\beta + 12\beta^2\right)\right)\right] \tag{15d}$$

In Figure 4a,b, the approximated solutions of the optimal parameters $\tilde{\nu}_{2,opt}(\nu_l)$ and $\tilde{\zeta}_{2,opt}(\nu_l)$ in Equations (14a) and (14b) are compared with those obtained numerically solving Equations (13a) and (13b) respectively, for several values of 13a-c μ_l. As can be seen from Figure 4, the approximated analytical solutions of the optimal parameters $\tilde{\nu}_{2,opt}(\nu_l)$ and $\tilde{\zeta}_{2,opt}(\nu_l)$ in Equations (14a) and (14b) closely agree with the numerical solution of Equation (13). Moreover, Figure 4 shows that the optimal parameter $\tilde{\nu}_{2,opt}(\nu_l)$ decreases for increasing values of μ_l, and both $\tilde{\nu}_{2,opt}(\nu_l)$ and $\tilde{\zeta}_{2,opt}(\nu_l)$ show an almost steady trend for $0.2 < \nu_l < 0.7$, suggesting that they are almost independent from μ_l in the range of practical interest.

Finally, optimal values of $\nu_{l,opt}$ that minimize the function $\phi_{X_b}(\zeta_2, \nu_l, \nu_2)$ can be found by solving Equation (13c). In this regard, in Figure 5, the trend of $\partial\phi_{X_b}(\zeta_2, \nu_l, \nu_2)/\partial\nu_l$ is depicted. As can be seen, a wide range of values of ν_l leads to values of $\partial\phi_{X_b}(\zeta_2, \nu_l, \nu_2)/\partial\nu_l$ close to zero, outside the neighbourhood of $\nu_l = 1$. Therefore, any choice of this parameter, in that wide range, approximately leads to the minimum of $\phi_{X_b}(\zeta_2, \nu_l, \nu_2)$, thus ultimately to the minimum of the base displacement variance $\sigma^2_{X_b}$.

In addition, the value of ν_l is strictly related to the total length of the liquid inside the container L ($\nu_l = \sqrt{2g/\omega_b^2 L}$), which is normally fixed by design constraints. Note that, considering the length (generally $L > 5m$) usually adopted for the design of these liquid tanks in real applications and the range of frequency of a common base-isolated structure, a plausible range of values for ν_l can be set between 0.2 and 0.7. In this range of practical interest, hence, a proper value of $\nu_{l,opt}$ can be chosen by setting

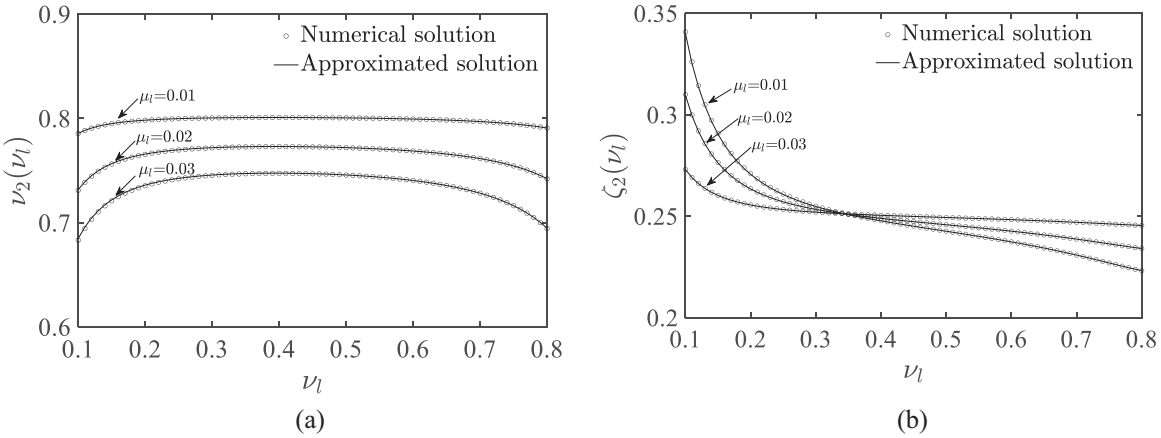

FIGURE 4 Approximated solutions (Equations 14a and 14b) versus numerical solutions (Equations 13a and 13b) for different values of μ_l ($\alpha = 0.9$, $\delta = 0.01$, $\beta = 0.3$): a) $\tilde{\nu}_{2,opt}(\nu_l)$; b) $\tilde{\xi}_{2,opt}(\nu_l)$

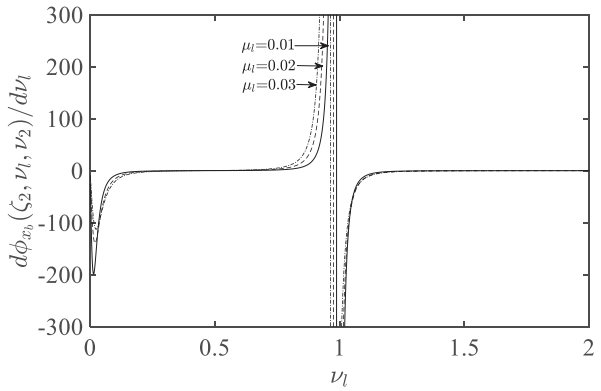

FIGURE 5 Values of ν_l, which minimize the objective function $\phi_{X_b}(\zeta_2, \nu_l, \nu_2)$ according to Equation (13c) for different values of μ_l (for $\alpha = 0.9, \beta = 0.3, \zeta_s = 0.01$)

a design value of the length L. Clearly, once the value of $\nu_{l,opt}$ is determined, Equations (14a) and (14b) can be used for a straightforward determination of the optimal TLCDI parameters.

As regards the determination of the optimal head loss coefficient, as already explained in Section 2.1, classical procedures determine the equivalent damping ratio ζ_l by employing a time-consuming iterative scheme. An accurate estimation of ζ_l can be performed by considering the variance of the BI system with the TLCDI in Equation (6), this time including the equivalent damping ratio ζ_l, following the procedure described in Appendix B. However, once the input structural parameters and the optimal values of $\tilde{\nu}_{2,opt}(\nu_l)$ and $\tilde{\xi}_{2,opt}(\nu_l)$ derived from Equations (14a) and (14b) have been set, again, a numerical minimization of the variance would be required to achieve an optimal value of ζ_l. Conversely, this study proposes an alternative quicker method for an approximate estimation of ζ_l. Specifically, the evaluation of the optimal value of ζ_l is obtained according to the analysis developed by Di Matteo et al. (2022) considering the BI structure with a classical TLCD subjected to a white noise excitation. In this case, the BI system displacement and the fluid velocity variances can be expressed as (Di Matteo et al., 2018):

$$\tilde{\sigma}^2_{X_b} = \tilde{\phi}_{X_b} \frac{\pi G_0}{4\,\omega_b^3}; \tilde{\sigma}^2_{\dot{U}} = \tilde{\phi}_{\dot{U}} \frac{\pi G_0}{4\,\omega_l}; \tag{16ab}$$

where $\tilde{\phi}_{X_b} = \tilde{N}_{X_b}/\tilde{D}_{X_b}$ and $\tilde{\phi}_{\dot{U}} = \tilde{N}_{\dot{U}}/\tilde{D}_{\dot{U}}$ with the numerators and denominators given by

$$\begin{aligned}
&\tilde{N}_{X_b} = \zeta_l\left(1+\mu_l-\alpha^2\mu_l\right)^2 + \nu_l\zeta_b\left[\alpha^4\mu_l^2 + 4\zeta_l^2(1+\mu_l)^2\right] + \\
&+ \nu_l^2\zeta_l(1+\mu_l)^2\left[4\zeta_b^2 - 2 - 2\,\mu_l + 3\alpha^2\mu_l + 4\zeta_l^2 + \right. \\
&\left.+4\zeta_l^2\mu_l\right] + \nu_l^3\zeta_b(1+\mu_l)^2\left(\alpha^2\mu_l + 4\zeta_l^2 + 4\zeta_l^2\mu_l\right) + \\
&+ \nu_l^4\zeta_l(1+\mu_l)^4; \\
&\tilde{D}_{X_b} = \zeta_b\zeta_l + \nu_l\zeta_l^2\left(4\zeta_b^2 + \alpha^2\mu_l\right) + 2\nu_l^2\zeta_b\zeta_l\mu_l\left[2\zeta_b^2 - 1 + \right. \\
&\left.+\left(\alpha^2-1\right) + 2\zeta_l^2(1+\mu_l)\right] + \nu_l^3\zeta_b^2\left[\alpha^2\mu_l + \right. \\
&\left.+ 4\zeta_l^2(1+\mu_l)\right] + \nu_l^4\zeta_b\zeta_l(1+\mu_l)^2; \\
&\tilde{N}_{\dot{U}} = \zeta_b + \nu_l\zeta_l\left(1 + 4\zeta_b^2 + \mu_l\right) + \nu_l^2 4\zeta_b^3; \\
&\tilde{D}_{\dot{U}} = \zeta_b\zeta_l + \nu_l\zeta_l^2\left(4\zeta_b^2 + \alpha^2\mu_l\right) + 2\nu_l^2\zeta_b\zeta_l\left[2\zeta_b^2 - 1 + \right. \\
&\left.+\left(\alpha^2-1\right)\mu_l + 2\zeta_l^2(1+\mu_l)\right] + \nu_l^3\zeta_b^2\left(\alpha^2\mu_l + 4\zeta_l^2 + \right. \\
&\left.+ 4\zeta_l^2\mu_l\right) + \nu_l^4\zeta_b\zeta_l(1+\mu_l)^2;
\end{aligned} \tag{17}$$

Considering the optimal values $\tilde{\nu}_{2,opt}(\nu_l)$ and $\tilde{\xi}_{2,opt}(\nu_l)$ found in Equations (14a) and (14b) and by minimizing the variance in Equation (16a) of the BI system equipped with TLCD, the optimal value of the equivalent damping ratio ζ_l can be obtained, without any iteration, thus resulting in a significant reduction in computational effort. Next, by setting this value in the expression of the fluid velocity variance, the value of $\tilde{\xi}_{opt}$ can be evaluated from

$$\tilde{\xi}_{opt} = 2L\zeta_{l,opt}\nu_{l,opt}\omega_b\sqrt{\pi/\left(2\tilde{\sigma}_{\dot{U}}\right)} \tag{18}$$

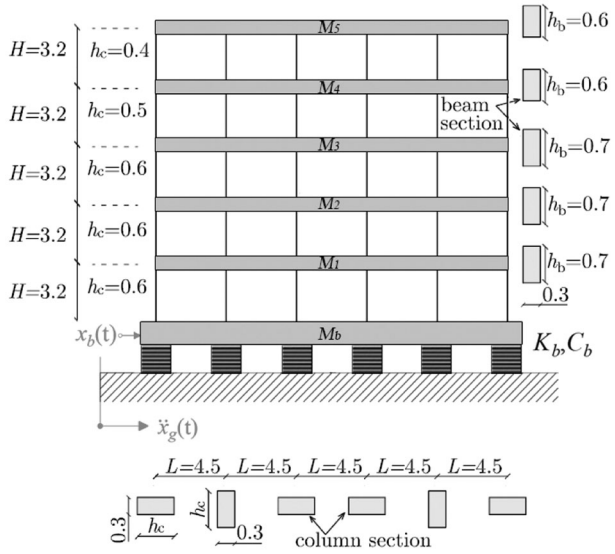

FIGURE 6 Benchmark model: Five story base-isolated structure (De Domenico & Ricciardi, 2018a)

As it will be shown in the next Section 4, this approach leads to almost identical results in terms of base displacement variance, compared to the classical iterative procedures without affecting the effectiveness of the TLCDI.

4 | OPTIMAL DESIGN PARAMETERS

The primary benefit of the proposed simplified approach is the straightforward evaluation of the optimal design parameters. To demonstrate its accuracy, a comparison is made here with the optimal values obtained by a numerical iterative procedure considering the original MDOF isolated structure. In particular, the benchmark structure considered is the base-isolated five-story planar frame ($n = 5$) previously studied by De Domenico and Ricciardi (2018a) and illustrated in Figure 6. The first four stories of the planar frame have a lumped mass of $M_j = 6 \cdot 10^4$ kg (for $j = 1, \dots, n-1$), and the mass of the fifth floor is $M_5 = 5 \cdot 10^4$ kg. The natural frequencies of this structure are given as $\omega_i[\text{rad/s}] = [12.5, 33.2, 56.1, 79.5, 112.2]$ ($i = 1, \dots, n$). The superstructure is a classically damped system with the damping ratio the same for each mode: $\zeta_i = 0.02$. The mass, natural frequency, and damping ratio of the BI subsystem are $M_b = M_5$, $\omega_b = \pi$ rad/s, $\zeta_b = 0.1$, respectively. Moreover, to calculate the base displacement variance in Equation (6), the PSD intensity is set to $G_0 = 0.002$, corresponding to an approximative peak ground acceleration of 0.02 g (Kaul, 1978).

The seismic performance of this base-isolated structure is evaluated in comparison to the same structure with the TLCDI. For this value of PSD and for this kind of structure, according to the closed-form solutions in Equations (14a) and (14b), the optimal TLCDI design parameters $\nu_{2,opt}$, $\xi_{2,opt}$, and $\tilde{\xi}_{opt}$ have been calculated by assuming that the liquid inside the TLCDI is water ($\rho = 997$ kg/m^3), the length ratio is $\alpha = 0.9$ (Wang et al., 2020a) with the total length $L = 10m$, $\mu_l = 0.04$, the mass ratio of the water tank δ is fixed to 1% and the inertance ratio $\beta = 0.3$ (De Domenico & Ricciardi, 2018a; Di Matteo et al., 2019). It is worth noting that the optimal parameters in Equations (14a) and (14b) do not depend on ζ_b, ζ_s, and G_0; hence, they are assumed constant when these parameters vary. Therefore, since these parameters have been previously neglected to achieve the proposed approximate expressions of the TLCDI parameters, the reliability of the proposed formulation might be mainly jeopardized when these parameters assume relatively high values. Moreover, as previously discussed, in the aforementioned expressions for the optimal parameters, the optimal frequency ratio of the liquid $\nu_{l,opt}$ can be set within a wide range of values, which might be rather different from each other according to the feasible lengths of the liquid tank L.

Therefore, a parametric analysis has been performed to verify the influence of ζ_b, ζ_s, L and G_0. Each one of them has been varied over a wide range of plausible values greater than zero since they cannot take negative values. Based on practical considerations, the constraints on the considered variables are the following: $L \in [1, 80], G_0 \in [0.001, 0.03], \zeta_b, \zeta_s \in [0.01, 0.3]$.

As customary in the literature, the numerical solution can be obtained by performing a control algorithm. In this respect, a single-objective genetic algorithm (GA) method (Goldberg & Holland, 1988; Kim & Roschke, 2006) has been used to find those values of $\tilde{\nu}_{2,opt}$, $\tilde{\xi}_{2,opt}$, and $\tilde{\xi}_{opt}$ that minimize the base displacement variance of the complete nonlinear system in Equation (2). The GA is often the preferred choice over many other optimization methods since, by applying the mechanisms of crossover, recombination, and mutation present in genetics, the solution is searched in multiple directions avoiding entrapment in local minima (Li & Adeli, 2018). A comprehensive review of control algorithms used primarily for vibration control is presented in (Gutierrez Soto & Adeli, 2017).

Clearly, the implementation of this numerical minimization algorithm requires some constraints on the sought TLCDI optimal parameters. Optimal values of $\tilde{\nu}_{2,opt}$, and $\tilde{\xi}_{2,opt}$ are sought in the range 0.01–1, while the boundary conditions for the head loss coefficient are chosen according to the experimental data of Wu et al. (2005) and the damping ratio is limited to the maximum value of $\zeta_l = 1$ (Di Matteo et al., 2015). It should be emphasized that in this procedure, each iteration of the GA algorithm yields an optimal value of ξ_{opt}, and the SLT

must be iteratively applied to evaluate the equivalent linear damping ratio ζ_l. Therefore, a cumbersome numerical procedure must be implemented in this case. With reference to the previously considered structural parameters, the optimal design parameters $\tilde{\nu}_{2,opt}$, $\tilde{\zeta}_{2,opt}$, and $\tilde{\xi}_{opt}$ determined through the proposed direct approach have been used to compute the base displacement variance $\sigma^2_{X_b}$ of the system as in Equation (5).

Next, the normalized displacement variance of the BI structure with TLCDI, denoted as $\varepsilon_{X_b} = \sigma^2_{X_b}/\sigma^2_{X_0}$, where $\sigma^2_{X_0}$ the BI displacement variance of the system without TLCDI, is evaluated. Note that this parameter may represent also a performance control index since lower values of ε_{Xb} indicate higher control efficacy of the TLCDI. The discrepancies between the normalized displacement variance obtained by the complete numerical GA procedure (dashed line) and that one calculated with the proposed analytical solutions of the optimal TLCDI parameters (dots) are shown in Figure 7 for different values of G_0, L, ζ_b, and ζ_s. Considering the fact that these errors are less than 2%, the proposed optimization method can be viewed as practically equivalent to the GA method in terms of control performance parameters. It is worth mentioning that the numerical approach is performed on the original system, which is a general linear damped MDOF base-isolated structure with the dynamic behavior governed by Equation (3). Hence, since a system with many degrees of freedom is considered, compared to the system in Equation (6) and the damping of the base isolation system is taken into account, minimizing the integral in Equation (5) requires many hours of computation time. Moreover, this numerical algorithm must be adapted to the new structural configuration for each possible variation of each parameter and performed again, unlike the proposed approach that provides a direct formula that can be used for the design of the TLCDI. Therefore, considering the large computational gain achieved by the proposed approximate formulation, it can be concluded that the analytical expressions provided in Equations (14a) and (14b) are a potent and reliable tool for the optimal design of the TLCDI.

In order to further investigate the potential of the TLCDI to represent a low-mass passive control strategy, the influence of the inertance on normalized variance ε_{Xb} has been studied. In this regard, ε_{Xb} is illustrated in Figure 8 as functions of the inertance ratio β and for different values of the liquid mass ratio μ_l. The results of Figure 8 reveal that, in accordance with the literature on other types of devices with the inerter (De Domenico & Ricciardi, 2018a), a certain value of inertance ratio ($\beta > 0.6$), increasing values of β lead to better performance ε_{Xb} by resorting to a smaller quantity of liquid mass.

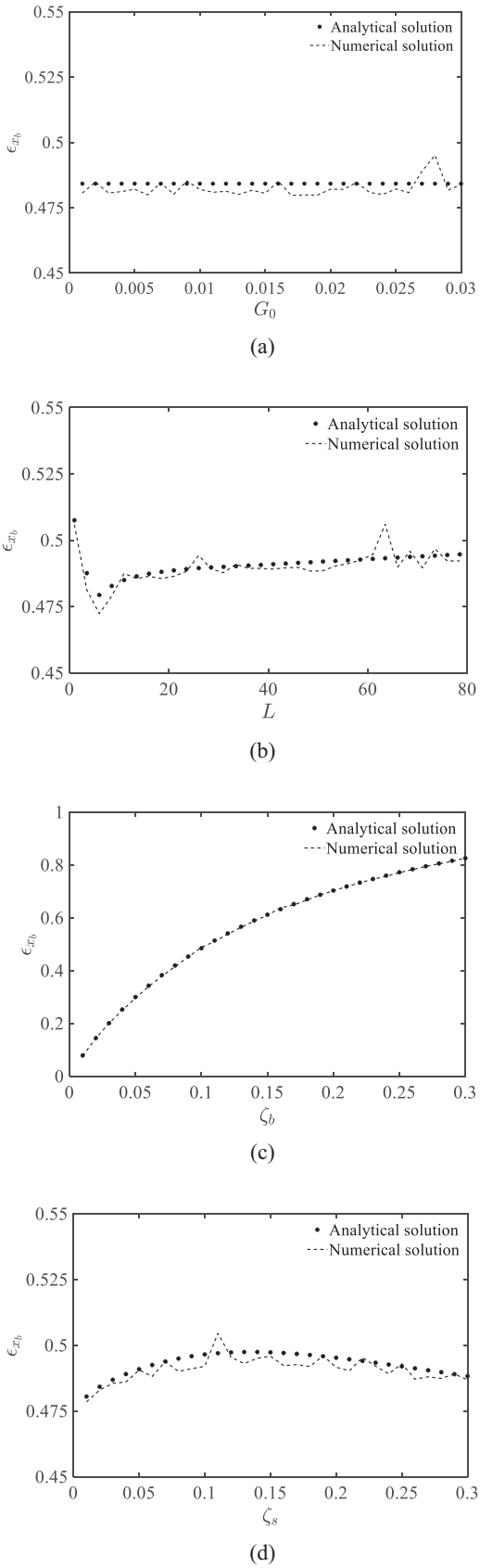

FIGURE 7 Normalized displacement variance: comparison between the numerical genetic algorithm procedure (dashed line) and the proposed formulation (dots) for different parameters

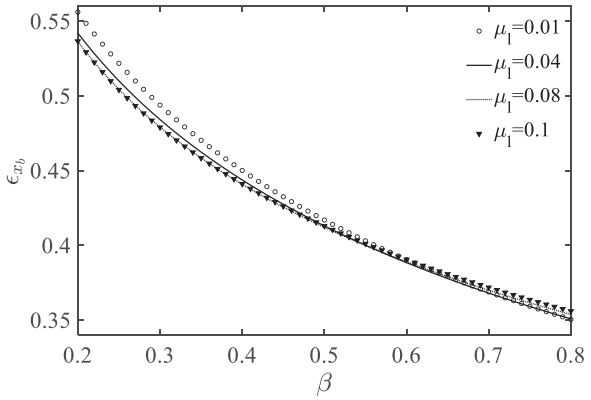

FIGURE 8 The effect of inertance on the normalized displacement variance of the base-isolation (BI) system with TLCDI

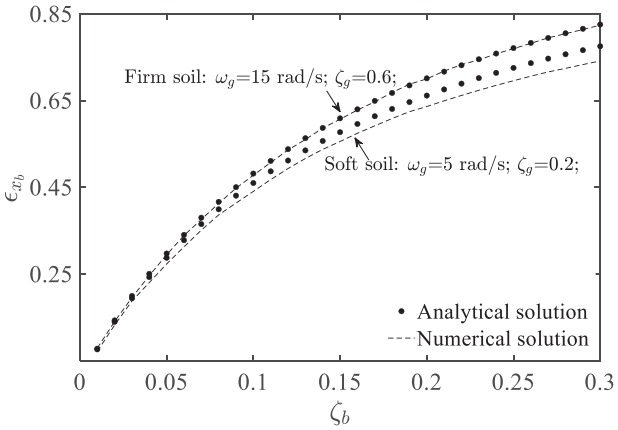

FIGURE 9 Performance control index ε_{X_b} in case of Kanai–Tajimi stationary filtered white noise process for different BI sub-system damping ratios: analytical solution (dots) versus numerical solution (dashed line)

The greater increase of ε_{Xb} with a large mass ratio for high β-values seems unusual, compared to traditional devices such as TMDs and TLCDs. This phenomenon is frequently observed when an inerter is used in combination with a secondary mass as discussed in the literature (De Domenico & Ricciardi, 2018a). The apparent reduction of ε_{Xb} for increasing values of β confirms that the inclusion of the inerter can lead to better performance. The additional inerter mechanism in the TLCDI greatly enhances the efficiency of the classical TLCD and makes the TLCDI an appealing, lightweight control device with superior control performance, compared to conventional TLCDs. In the literature, a value of inertance between 0.3 and 0.5 is usually suggested as a good compromise between cost-effectiveness and performances (De Domenico & Ricciardi, 2018a, Abdeddaim et al., 2020).

The results presented above were derived considering a Gaussian white noise with zero mean for modeling ground acceleration, whose properties allowed obtaining approximate expressions for the optimal TLCDI parameters. Therefore, with the aim of proving the validity of Equations (14a) and (14b) also in the case of more general broad-band earthquake excitation, a further analysis was carried out. For this purpose, the widely used Kanai–Tajimi stationary filtered process is adopted as a more realistic model of earthquake ground acceleration. This process is characterized by the following one-sided PSD (Tajimi, 1960).

$$G_{\ddot{X}_g}(\omega) = G_0 \frac{\omega_g^4 + 4\zeta_g^2\omega_g^2\omega^2}{\left(\omega_g^2 - \omega^2\right)^2 + 4\zeta_g^2\omega_g^2\omega^2} \tag{19}$$

where G_0 is the constant white noise PSD whose value is related to the bedrock peak ground acceleration according to Kaul (1978), while ω_g and ζ_g are the soil natural frequency and damping ratio. The corresponding variance of the base isolation sub-system $\sigma^2_{X_b}$ is given as (Roberts & Spanos, 1990)

$$\sigma^2_{X_b} = \int_0^\infty |H_{X_b}(\omega)|^2 G_{\ddot{X}_g}(\omega)\, d\omega \tag{20}$$

A closed form of this variance can be obtained in a similar manner to the case of white noise input as explained in Appendix B. However, since long and unwieldy closed-form solutions would be achieved for this model, a numerical minimization procedure is again pursued to find the optimal TLCDI design parameters that reach the minimum of Equation (20). Once these optimized parameters are obtained by the numerical approach, the corresponding performance control index ε_{X_b} is evaluated and compared with the pertinent values obtained with the optimal parameters in Equations (14a) and (14b). For the sake of conciseness, results are shown in Figure 9 only for ζ_b varying between 0 and 0.3 and for two different soil conditions.

As it can be seen, even assuming a non-white earthquake excitation, the performance control index obtained with the optimal values in Equations (14a) and (14b) (based on a white noise process) largely agrees with the value obtained with the complete solution, with a slight discrepancy for the soft soil type. Considering the significant reduction in computational effort achieved by the proposed analytical solution and the small deviations in terms of ε_{X_b}, the above approach again proves to be a powerful and reliable tool for the efficient estimation of the TLCDI design parameters.

5 | CONTROL PERFORMANCE

The above-proposed optimization procedure has been derived considering a white noise base excitation, thus leading with the minimal computational cost to the simplified analytical expressions in Equations (14a) and (14b) for the TLCDI optimal parameters. However, the assumption of stationarity and a constant PSD represents an idealized model that does not take into account the real nature of earthquakes. In light of this, to test the reliability of the proposed analytical expressions when exposed to real ground motions, 44 records of past seismic events selected from the Federal Emergency Management Agency (FEMA) P-695-FF record set (FEMA P-695, 2009) were applied as the base excitation for the numerical simulations. For completeness, to account for structures with different properties, numerical simulations were performed on two base-isolated frame structures with different numbers of floors, characterized by different mass, stiffness, and damping parameters. The first case study is the same structure already analyzed in Section 4, whereas the second structure is a base-isolated high-rise building with 20 stories (Ma et al., 2014).

In addition to the seismic analysis of the system with TLCDI, the dynamic response of the uncontrolled BI system and the BI system equipped with a conventional TLCD were computed for comparison. The parameters of the TLCD with the same mass and length as the TLCDI were optimized according to a procedure presented in Di Matteo et al. (2018). In these analyses, the coupled nonlinear differential equations of motion (Equation 2 in the case of the BI system with TLCD) were solved using a fourth-order Runge–Kutta algorithm. For each of the 44 recorded ground motions, the displacement relative to the ground, total acceleration, and interstory drift ratio were determined for the BI structure, the BI structure equipped with the TLCDI and the one controlled by the conventional TLCD.

As a result of these analyses, Figure 10 shows a comparison of the profiles of the median (line with circle markers) of the peak response quantities of the five-story BI structure without a control device (black dotted line), with TLCD (blue dash-dotted line) and with TLCDI optimized via the approximated solution (red solid line). The 16th (marked with crosses) and 84th (marked with squares) percentile values are shown as a measure of dispersion (Ibarra & Krawinkler, 2005). Since the record-to-record variability of the seismic response is in general more or less log-normally distributed, the distribution of the considered response quantity is completely captured by its median,

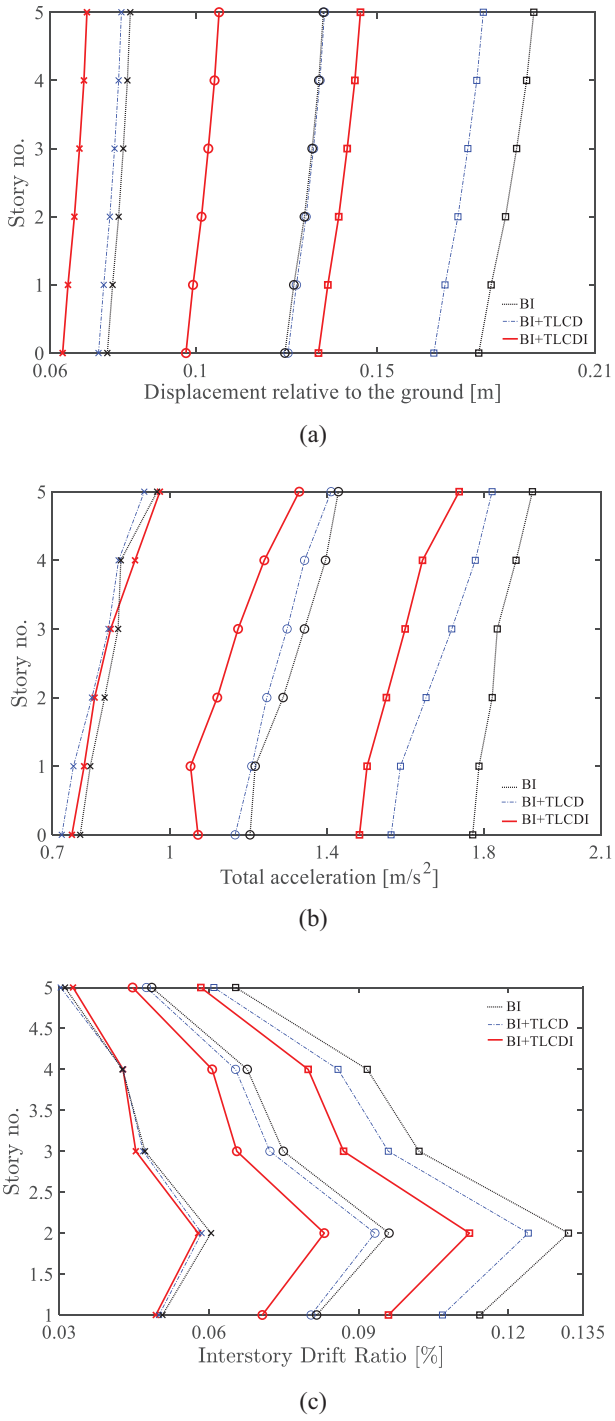

FIGURE 10 Response profiles of the five-story BI structure with TLCDI designed with the proposed optimization procedure (red solid line), BI structure with TLCD (blue dash-dotted line), and BI structure (black dotted line) subjected to the 44 ground motion records of the FEMA P-695-FF set: circles-median; crosses-16th percentile; squares-84th percentiles. (a) Peak floor displacement relative to the base; (b) Peak floor total acceleration; (c) Peak floor interstory drift ratio

16th and 84th percentile value, as explained, for instance, in Limpert et al. (2001).

Figure 10 demonstrates that both devices are able to mitigate the seismic response of the BI system. However, the optimized TLCDI device in combination with the BI subsystem results in displacements (Figure 10a) and total accelerations (Figure 10b) of the BI system that is always lower than the corresponding values of the BI system with the conventional TLCD. In particular, the median of the peak displacement and acceleration of the isolation floor is decreased by 22% and 11%, respectively, when the BI structure is controlled with a TLCDI, compared to the plain base-isolated structure. It should be noted that this reduction is not achieved at the expense of increased interstory drift ratios (see Figure 10c) as it may happen when adopting strategies based on the amplification of the damping of the BI subsystem (Kelly, 1999). Thus, the beneficial features of BI systems are retained even when employing the TLCDI.

In this regard, Figure 11 shows the comparison of the response time histories, in terms of base displacement (Figure 11a,b) and roof displacement relative to the ground (Figure 11c–d), of the five-story BI benchmark structure with TLCDI, with TLCD, and without any device subjected to two records of the FEMA P-695-FF 44 with different features, namely, the Kocaeli and the Duzce ground motions. As can be seen, the TLCDI device is particularly effective in reducing the BI displacement for both records with a significant reduction of the peak BI displacement of almost 45% for the Kocaeli earthquake (Figure 11a) and 30% for the Duzce earthquake (Figure 11b), whereas the TLCD provides a reduction of 9% and 3%, respectively, compared to the peak responses of the BI system.

Similar results are also observed in the roof floor displacements relative to the base, as depicted in Figure 11c,d, where the TLCDI reduces the peak floor displacements up to 34% for the Kocaeli earthquake (Figure 11c), compared to the 12% achieved by the conventional TLCD. As can be seen, both TLCDI and TLCD have little effect on the structural response in the first few seconds of the excitation as is common with passive control devices. For an earlier response suppression, the use of an active system device or a sort of accelerated device is recommended (Lin et al., 2010; Tsai, 1995).

Nevertheless, Figure 11 confirms that coupling a TLCDI designed with the proposed approach with a BI system can effectively reduce the BI displacements, as well as other response quantities such as floor displacements, compared to the system without TLCDI or with the conventional TLCD.

For a better understanding, it is also worth taking a view on the energy. In this regard, Figure 12a,b shows the input energy and the dissipated energy for both the

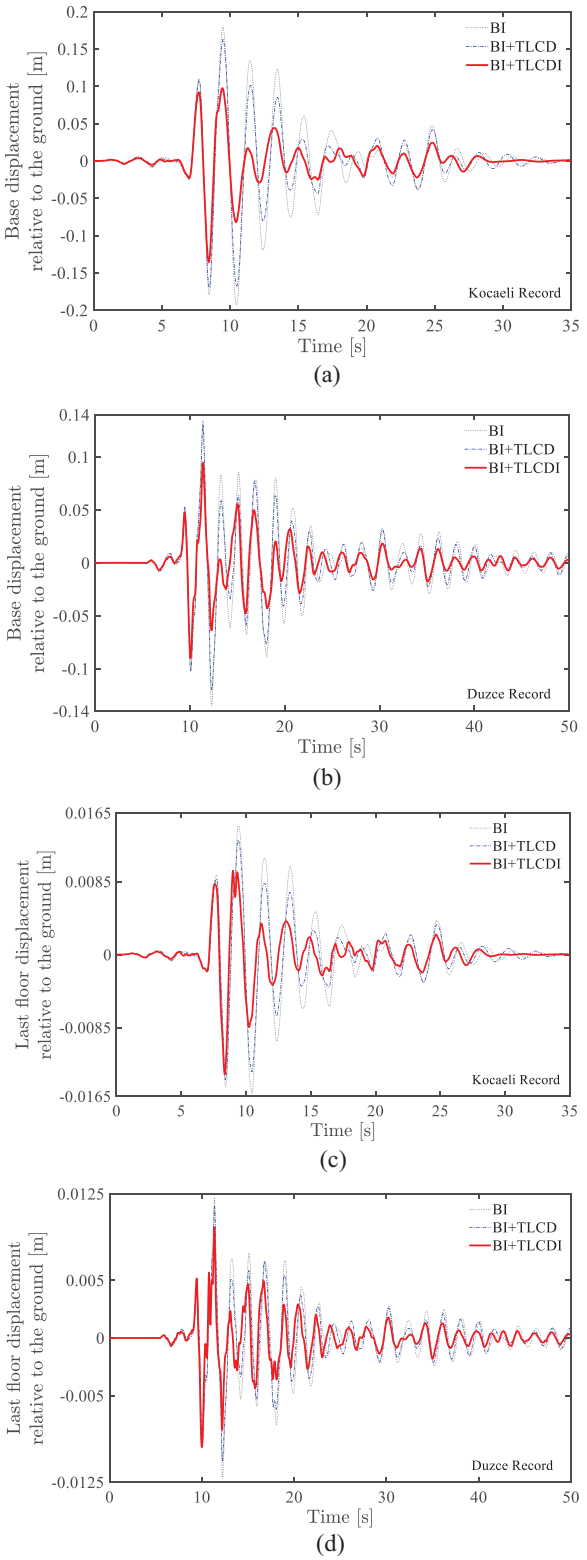

FIGURE 11 Response in terms of BI displacement relative to the ground induced by the (a) Kocaeli record; (b) Duzce record; response in terms of roof displacement relative to the ground induced by the (c) Kocaeli record; (d) Duzce record. Five-story BI structure with TLCDI – red solid line, five-story BI structure with TLCD–blue dash-dotted line, five-story BI structure without device–black dotted line

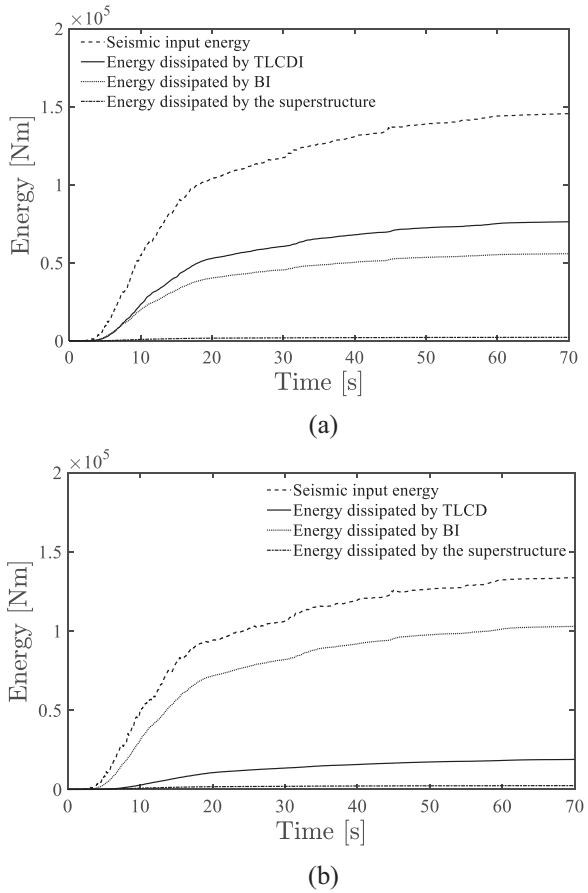

FIGURE 12 Comparison on energy contributions time-history for: (a) Five-story BI structure with TLCDI; (b) five-story BI structure with TLCD

BI system with TLCDI and the BI system with conventional TLCD. Specifically, the mean of the cumulative dissipation energy terms contributing to the total input energy (De Domenico & Ricciardi, 2018b) during the 44 ground motion records is presented. In the TLCDI system (Figure 12a), the dissipated energy provided by the TLCDI damper and liquid motion is reasonably high (53% of dissipation), compared to the energy dissipated by the stand-alone BI system (38%). On the contrary, as observed in Figure 12b, the energy dissipated by the TLCD (14%) is lower than the energy dissipated by the BI system (75%). Note a similar result was found in studies considering a BI system with TMDI and with TMD (De Domenico & Ricciardi, 2018b). Therefore, compared to the case with TLCD, the energy stored in the isolators decreases for BI systems endowed with the TLCDI, confirming the remarkable influence of the inerter on protecting the BI system from undesirable vibrations.

To further verify the reliability of the simplified optimization procedure, the study on the TLCDI control performance is extended to the case of the high-rise base-isolated building with 20 stories studied in Ma et al. (2014). The mass and stiffness properties of the superstructure are different depending upon the story number. Specifically, the lumped masses at each story are: $M_j = 27.6 \cdot 10^3 kg$ (for $j = 1 \div 8$), $M_j = 24.1 \cdot 10^3 kg$ (for $j = 9 \div 16$) and $M_j = 20.7 \cdot 10^3 kg$ (for $j = 17 \div 20$), while the mass of the BI subsystem is $M_b = 34.4 \cdot 10^4 kg$. The damping ratios of the superstructure and isolation slab are $\zeta_i = 0.03$ and $\zeta_b = 0.1$, respectively; the fundamental frequency of the superstructure is $\omega_{s,1} = 3.78 \text{rad/s}$, and of the base-isolated system is $\omega_b = 1.80 \text{rad/s}$.

The response profiles of this structure subjected to the 44 ground motion records of the FEMA P-695-FF set are shown in Figure 13. For this case study, a comparison with the BI system equipped with a TMDI having equal mass and inertance ratios as the TLCDI (and optimized as in Di Matteo et al., 2019) has been also investigated. Similar conclusions can be made for this structure by examining the displacements relative to the ground in Figure 13a. As can be seen, the most efficient control is attained by the BI system equipped with the TLCDI (red solid line) and the TMDI (green dashed line), while the BI system with TLCD (blue dash-dotted line) shows a performance comparable to that of the stand-alone BI structure (black dotted line). Furthermore, a slight improvement in the interstory drift ratio shown in Figure 13c by the TLCDI and the TMDI, compared to the TLCD, is observed. In this case, the discontinuities in the interstory drifts at the eighth and 16th floors are due to stiffness changes in the superstructure (Ma et al., 2014). On the other hand, as far as the acceleration profiles are concerned, the BI + TLCDI configuration may lead to detrimental effects as illustrated in Figure 13b. In fact, a small increase in the median and the 16th percentile of the peak accelerations is observed for the BI system with TLCDI. Once again, the BI system with TMDI leads to overlapping data with respect to the TLCDI indicating that their use can be interchangeable for the purpose of this study depending on the design requirements.

This effect of increased accelerations, shown by both TMDI and TLCDI, can be attributed to the remarkable contribution of higher modes of vibration to the seismic response of this high-rise structure. Specifically, as discussed in Ma et al. (2014), higher modes have a substantial effect on the seismic accelerations of the superstructure while having a small impact on the response of the base slab and the drift.

It is worth pointing out that these results are consistent with the fact that the proposed optimization procedure was developed under the assumption that the superstructure is a single rigid mass, and thus focuses on the seismic response of the first vibration mode that usually dominates the response of low base-isolated structures.

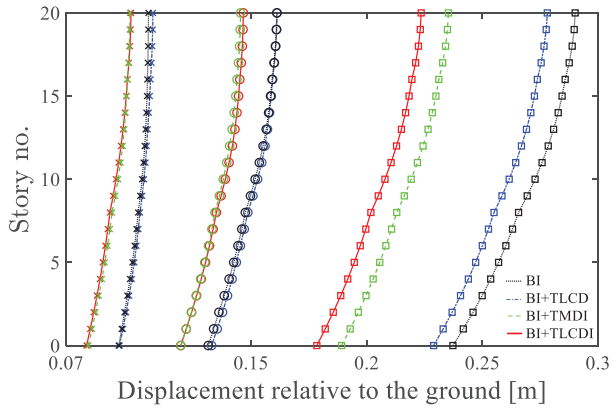

(a)

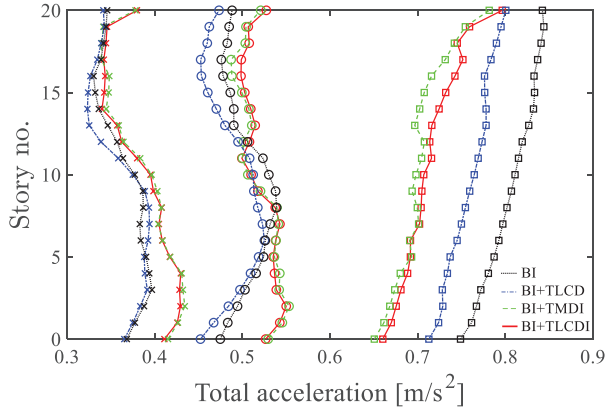

(b)

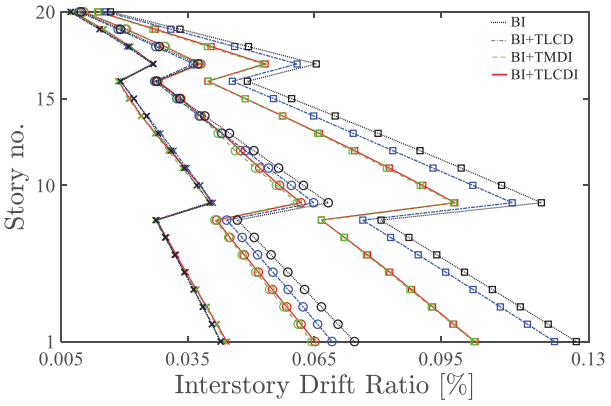

(c)

FIGURE 13 Response profiles of the 20-story BI structure with TLCDI designed with the proposed optimization procedure (red solid line), 20-story BI structure with TMDI (green dashed line), with TLCD (blue dash-dotted line) and BI structure (black dotted line) subjected to the 44 ground motion records of the FEMA P-695-FF set: circles-median; crosses-16th percentile; squares-84th percentiles. (a) Peak floor displacement relative to the base; (b) Peak floor total acceleration; (c) Peak floor interstory drift ratio

Moreover, the results in Figure 13a indicate that the effectiveness of the proposed approach, formulated with the single objective of reducing the base displacement, is still preserved for this purpose even when isolated high-rise buildings are considered.

However, when a considerable number of higher modes contribute to the dynamic response of the superstructure, as in this case, the implementation of a multi-objective optimization procedure or the resort to active control devices may be more of an appropriate strategy.

In this regard, a multi-objective optimization aimed at simultaneously reducing the higher mode acceleration may lead to better overall control. On the other hand, active or semiactive TLCDs, for example, by varying the optimal value of the head loss coefficient according to the frequency content of the external force, may be able to reduce the response at each natural frequency (Kim & Adeli, 2005b). Although these strategies may be considered more suitable to cover a wide range of excitation, the proposed passive configuration of TLCD with inerter is more convenient and inherently reliable for controlling those structures whose response is dominated by one main mode (El-Khoury & Adeli, 2013), such as most base-isolated structures, since it does not rely on an external energy source.

6 | CONCLUSION

This paper addressed the passive control effect of the TLCDI on the dynamic response of seismically excited base-isolated MDOF structures. The nonlinear equations of motion of the hybrid-controlled system were established, and the optimal design parameters of the TLCDI were studied in detail by means of the SLT and the Lyapunov equation. Approximate analytical expressions for the optimal TLCDI parameters were found by minimizing the variance of the base displacement considering a Gaussian white noise model of the base excitation and under some simplifying assumptions. The following main conclusions can be drawn from the results of this study:

1. The accuracy of these formulae was demonstrated by a comparative analysis with a conventional cumbersome numerical optimization procedure pursued when the previous assumptions are removed.
2. In particular, the proposed approach leads to almost identical results, compared to the numerical approach with a significant reduction in computational effort.

3. Seismic analyses carried out on two different base-isolated structures equipped with a TLCDI designed with the proposed approach have demonstrated the superior control performance of the TLCDI over a classical TLCD with the same liquid mass.

In summary, the results of the performed analyses demonstrated the reliability of the proposed optimization procedure even in the presence of recorded ground accelerations and proved that the TLCDI is a lightweight-based control tool that significantly improves the seismic performance of base-isolated structures.

ACKNOWLEDGEMENTS

The authors gratefully acknowledge the support received from the Italian Ministry of University and Research, through the PRIN 2017 funding scheme (project 2017J4EAYB 002–Multiscale Innovative Materials and Structures "MIMS").

REFERENCES

Abdeddaim, M., Djerouni, S., Ounis, A., & Nassim, D. (2020). Double tuned mass damper inerter for seismic response reduction of structures. *EASD Procedia EURODYN*, Athens, Greece (pp. 1433–1444).

Adam, C., Di Matteo, A., Furtmüller, T., & Pirrotta, A. (2017). Earthquake excited base-isolated structures protected by tuned liquid column dampers: Design approach and experimental verification. *Procedia Engineering*, *199*, 1574–1579.

Aldemir, Ü., Yanik, A., & Bakioglu, M. (2012). Control of structural response under earthquake excitation. *Computer-Aided Civil and Infrastructure Engineering*, *27*(8), 620–638.

Amezquita-Sanchez, J. P., Park, H. S., & Adeli, H. (2017). A novel methodology for modal parameters identification of large smart structures using MUSIC. *Empirical Wavelet Transform, and Hilbert Transform. Engineering Structures*, *147*, 148–159.

Banerji, P., Murudi, M., Shah, A. H., & Popplewell, N. (2000). Tuned liquid dampers for controlling earthquake response of structures. *Earthquake Engineering & Structural Dynamics*, *29*(5), 587–602.

Banerji, P., & Samanta, A. (2011). Earthquake vibration control of structures using hybrid mass liquid damper. *Engineering Structures*, *33*(4), 1291–1301.

Crandall, S. H., & Mark, W. D. (1963). *Random vibration in mechanical systems*. Academic Press.

De Domenico, D., & Ricciardi, G. (2018a). An enhanced base-isolation system equipped with optimal tuned mass damper inerter (TMDI). *Earthquake Engineering & Structural Dynamics*, *47*(5), 1169–1192.

De Domenico, D., & Ricciardi, G. (2018b). Optimal design and seismic performance of tuned mass damper inerter (TMDI) for structures with nonlinear base isolation systems. *Earthquake Engineering & Structural Dynamics*, *47*, 2539.

Den Hartog, J. P. (1956). *Mechanical vibrations*. McGraw-Hill.

Di Matteo, A., Pirrotta, A., & Tumminelli, S. (2017). Combining TMD and TLCD: Analytical and experimental studies. *Journal of Wind Engineering and Industrial Aerodynamics*, *167*, 101–113.

Di Matteo, A., Furtmüller, T., Adam, C., & Pirrotta, A. (2018). Optimal design of tuned liquid column dampers for seismic response control of base-isolated structures. *Acta Mechanica*, *229*, 437–454.

Di Matteo, A., Lo Iacono, F., Navarra, G., & Pirrotta, A. (2014). Direct evaluation of the equivalent linear damping for TLCD systems in random vibration for pre-design purposes. *International Journal of Non-Linear Mechanics*, *63*, 19–30.

Di Matteo, A., Lo Iacono, F., Navarra, G., & Pirrotta, A. (2015). Optimal tuning of tuned liquid column damper systems in random vibration by means of an approximate formulation. *Meccanica*, *50*(3), 795–808.

Di Matteo, A., Masnata, C., Adam, A., & Pirrotta, A. (2022). Optimal design of tuned liquid column damper inerter for vibration control. *Mechanical Systems and Signal Processing*, *167*, 108553.

Di Matteo, A., Masnata, C., & Pirrotta, A. (2019). Simplified analytical solution for the optimal design of tuned mass damper inerter for base-isolated structures. *Mechanical Systems and Signal Processing*, *134*, 106337.

El-Khoury, O., & Adeli, H. (2013). Recent advances on vibration control of structures under dynamic loading. *Archives of Computational Methods in Engineering*, *20*(4), 353–360.

FEMA P-695 (2009). *Quantification of building seismic performance factors*. Technical Representative Federal Emergency Agency. FEMA P-695.

Furtmüller, T., Di Matteo, A., Adam, C., & Pirrotta, A. (2019). Base-isolated structure equipped with tuned liquid column damper: An experimental study. *Mechanical Systems and Signal Processing*, *116*, 816–831.

Ghaedi, K., Ibrahim, Z., Adeli, H., & Javanmardi, A. (2017). Recent developments in vibration control of building and bridge structures. *Journal of Vibroengineering (Invited Review)*, *19*(5), 3564–3580.

Goldberg, D. E., & Holland, J. H. (1988). Genetic algorithms and machine learning. *Machine Learning*, *3*, 95–99.

Gutierrez Soto, M., & Adeli, H. (2013). Tuned mass dampers. *Archives of Computational Methods in Engineering*, *20*(4), 419–431.

Gutierrez Soto, M., & Adeli, H. (2017). Recent advances in control algorithms for smart structures and machines. *Expert Systems*, *34*(2), e12205.

Gutierrez Soto, M., & Adeli, H. (2018). Vibration control of smart base-isolated irregular buildings using neural dynamic optimization model and replicator dynamics. *Engineering Structures*, *156*(1), 322–336.

Gutierrez Soto, M., & Adeli, H. (2019). Semi-active vibration control of smart isolated highway bridge structures using replicator dynamics. *Engineering Structures*, *186*, 536–552.

Hitchcock, P. A., Kwok, K. C. S., Watkins, R. D., & Samali, B. (1997). Characteristics of liquid column vibration absorbers (LCVA)—I. *Engineering Structures*, *19*(2), 126–134.

Hochrainer, M. J., & Ziegler, F. (2006). Control of tall building vibrations by sealed tuned liquid column damper. *Structural Control and Health Monitoring*, *13*(6), 980–1002.

Ibarra, L. F., & Krawinkler, H. (2005). *Global collapse of frame structures under seismic excitations*. Report No. PEER 2005/06. Berkeley, CA: Pacific Earthquake Engineering Research Center, University of California.

Javadinasab Hormozabad, S., Gutierrez Soto, M., & Adeli, H. (2021). Integrating structural control, health monitoring, and energy harvesting for smart cities. *Expert Systems*, *38*(8), e12845.

Kaul, M. K. (1978). Stochastic characterization of earthquakes through their response spectrum. *Earthquake Engineering & Structural Dynamics*, *6*, 497–509.

Kelly, J. M. (1990). Base-isolation: Linear theory and design. *Earthquake Spectra*, *6*, 223–244.

Kelly, J. M. (1997). *Earthquake-resistant design with rubber*. Springer Verlag.

Kelly, J. M. (1999). The role of damping in seismic isolation. *Earthquake Engineering & Structural Dynamics*, *28*, 3–20.

Kim, H., & Adeli, H. (2005a). Hybrid control of smart structures using a novel wavelet-based algorithm. *Computer-Aided Civil and Infrastructure Engineering*, *20*, 7–22.

Kim, H., & Adeli, H. (2005b). Wind-induced motion control of 76-story benchmark building using the hybrid damper-tuned liquid column damper system. *Journal of Structural Engineering*, *131*(12), 1794–1802.

Kim, H. S., & Roschke, P. N. (2006). Fuzzy control of base-isolation system using multi-objective genetic algorithm. *Computer-Aided Civil and Infrastructure Engineering*, *21*, 436–449.

Li, Z., & Adeli, H. (2018). Control methodologies for vibration control of smart civil and mechanical structures. *Expert Systems*, *35*(6), e12354.

Limpert, E., Stahel, W. A., & Abbt, M. (2001). Log-normal distributions across the sciences: Keys and clues. *BioScience*, *51*, 341–352.

Lin, C.-C., Chen, C.-L., & Wang, J.-F. (2010). Vibration control of structures with initially accelerated passive tuned mass dampers under near-fault earthquake excitation. *Computer-Aided Civil and Infrastructure Engineering*, *25*(1), 69–75.

Love, J. S., Tait, M. J., & Toopchi-Nezhad, H. (2011). A hybrid structural control system using a tuned liquid damper to reduce the wind induced motion of a base-isolated structure. *Engineering Structures*, *33*, 738–746.

Ma, C., Zhang, Y. H., Tan, P., & Zhou, F. L. (2014). Seismic response of base-isolated high-rise buildings under fully nonstationary excitation. *Shock and Vibration*, *2014*, 1–11.

Marian, L., & Giaralis, A. (2014). Optimal design of a novel tuned mass-damper–inerter (TMDI) passive vibration control configuration for stochastically support-excited structural systems. *Probabilistic Engineering Mechanics*, *38*, 156–164.

Masnata, C., Di Matteo, A., Adam, C., & Pirrotta, A. (2020). Smart structures through nontraditional design of Tuned Mass Damper Inerter for higher control of base-isolated systems. *Mechanics Research Communications*, *105*, 103513.

Masnata, C., Di Matteo, A., Adam, C., & Pirrotta, A. (2021). Assessment of the tuned mass damper inerter for seismic response control of base-isolated structures. *Structural Control Health Monitoring*, *28*, e2665.

Navarra, G., Lo Iacono, F., & Oliva, M. (2020). An efficient stochastic linearisation procedure for the seismic optimal design of passive control devices. *Frontiers in Built Environment*, *6*, 32.

Pandey, D. K., Mishra, S. K., & Chakraborty, S. (2022). A tuned liquid mass damper implemented in a deep liquid storage tank for seismic vibration control of short period structures. *Structural Design of Tall and Special Buildings*, *31*(810), e1928.

Roberts, J. B., & Spanos, P. D. (1990). *Random vibration and statistical linearization*. Dover Publications.

Smith, M. C. (2002). Synthesis of mechanical networks: The inerter. *IEEE Transactions on Automatic Control*, *47*(10), 1648–1662.

Smith, M. C. (2020). The inerter: A retrospective. *Annual Review of Control, Robotics, and Autonomous Systems*, *3*, 361–391.

Tait, M. (2008). Modelling and preliminary design of a structure-TLD system. *Engineering Structures*, *30*, 2644–2655.

Tajimi, H. (1960). A statistical method of determining the maximum response of a building structure during earthquake. *Proceedings of the 2nd World Conference on Earthquake Engineering*, Tokyo, Japan (pp. 781–798).

Takewaki, I., Murakami, S., Yoshitomi, S., & Tsuji, M. (2012). Fundamental mechanism of earthquake response reduction in building structures with inertial dampers. *Structural Control and Health Monitoring*, *19*(6), 590–608.

Taniguchi, T., Der Kiureghian, A., & Melkumyan, M. (2008). Effect of tuned mass damper on displacement demand of base-isolated structures. *Engineering Structures*, *30*(12), 3478–3488.

Tsai, H. C. (1995). The effect of tuned-mass damper on the seismic response of base-isolated structures. *International Journal of Solids and Structures*, *32*, 1195–1210.

Wang, L., Zhao, X., & Zheng, Y. M. (2016). A combined tuned damper and an optimal design method for wind-induced vibration control for super tall buildings. *The Structural Design of Tall and Special Buildings*, *25*, 468–502.

Wang, Q., Qiao, H., De Domenico, D., Zhu, Z., & Tang, Y. (2020b). Seismic response control of adjacent high-rise buildings linked by the Tuned Liquid Column Damper-Inerter (TLCDI). *Engineering Structures*, *223*, 111169.

Wang, Q., Tiwari, N. D., Qiao, H., & Wang, Q. (2020a). Inerter-based tuned liquid column damper for seismic vibration control of a single-degree-of freedom structure. *International Journal of Mechanical Sciences*, *184*, 105840.

Wu, J.-C., Shih, M.-H., Lin, Y.-Y., & Shen, Y.-C. (2005). Design guidelines for tuned liquid column damper for structures responding to wind. *Engineering Structures*, *27*(13), 1893–1905.

Xu, Y. L., Kwok, K. C. S., & Samali, B. (1992). The effect of tuned mass dampers and liquid dampers on cross-wind response of tall/slender structures. *Journal of Wind Engineering and Industrial Aerodynamics*, *40*(1), 33–54.

Yang, J. N., Danielians, A., & Li, S. C. (1991). Aseismic hybrid control systems for building structures. *Journal of Engineering Mechanics*, *117*, 836–853.

Zelleke, D. H., & Matsagar, V. A. (2010). Semi-active algorithm for energy-based predictive structural control using tuned mass dampers. *Computer-Aided Civil and Infrastructure Engineering*, *34*, 1010–1025.

Zhao, Z., Zhang, R., Jiang, Y., & Pan, C. (2019). A tuned liquid inerter system for vibration control. *International Journal of Mechanical Sciences*, *164*, 105171.

Zhu, F., Wang, J., Jin, F., & Lu, L. (2019). Control performance comparison between tuned liquid damper and tuned liquid column damper using real-time hybrid simulation. *Earthquake Engineering and Engineering Vibration*, *18*, 695–701.

How to cite this article: Masnata, C., Matteo, A. D., Adam, C., & Pirrotta, A. (2023). Efficient estimation of tuned liquid column damper inerter (TLCDI) parameters for seismic control of base-isolated structures. *Computer-Aided Civil and Infrastructure Engineering*, *38*, 1638–1656. https://doi.org/10.1111/mice.12929

APPENDIX A

This appendix presents the transfer functions in terms of displacements of the system in Equation (3) obtained by applying the Fourier transform as follows:

$$\begin{gathered}\mathbf{X}_s(\omega)\left(-\omega^2\mathbf{M}_s+i\omega\mathbf{C}_s+\mathbf{K}_s\right)-\omega^2\mathbf{M}_s\mathbf{r}X_b(\omega)\\=-\mathbf{M}_s\mathbf{r}\ddot{X}_g(\omega)\\X_b(\omega)\left[-\omega^2(1+\mu_t+\beta)+2i\omega\omega_b\zeta_b+\omega_b^2\right]\\-\frac{\omega^2\mathbf{r}^{\mathbf{T}}\mathbf{M}_s}{M_{tot}}\mathbf{X}_s(\omega)=\\=(\mu_t+\beta)\omega^2Y(\omega)+\alpha\mu_lU(\omega)-(1+\mu_t)\ddot{X}_g(\omega)\\Y(\omega)\left[-(\mu_t+\beta)\omega^2+2i\omega\omega_2\zeta_2\mu_t+\mu_t\omega_2^2\right]\\-\omega^2(\mu_t+\beta)X_s(\omega)=\\=\alpha\mu_l\omega^2U(\omega)-\mu_t\ddot{X}_g(\omega)\\U(\omega)\left[\omega^2+2i\omega\omega_l\zeta_l+\omega_l^2\right]-\omega^2\alpha X_s(\omega)-\omega^2\alpha Y(\omega)\\=-\alpha\ddot{X}_g(\omega)\end{gathered}\tag{A.1}$$

By definition of the functions

$$a(\omega)=-(1+\mu_t+\beta)\omega^2+2i\omega\omega_s\zeta_s+\omega_s^2$$

$$b(\omega)=-(\mu_t+\beta)\omega^2+2i\omega\omega_2\zeta_2\mu_t+\mu_t\omega_2^2\tag{A.2}$$

$$b(\omega)=-(\mu_t+\beta)\omega^2+2i\omega\omega_2\zeta_2\mu_t+\mu_t\omega_2^2$$

$$\mathbf{d}(\omega)=\left[-\omega^2\mathbf{M}_s+i\omega\mathbf{C}_s+\mathbf{K}_s\right]^{-1}$$

the BI displacement transfer function $H_{X_b}(\omega)=X_b(\omega)/\ddot{X}_g(\omega)$ of the system with TLCDI, the container displacement $H_Y(\omega)=Y(\omega)/\ddot{X}_g(\omega)$, the liquid column transfer functions, $H_U(\omega)=U(\omega)/\ddot{X}_g(\omega)$, and the superstructure displacement transfer function $H_{\mathbf{X}_s}(\omega)=\mathbf{X}_s(\omega)/\ddot{X}_g(\omega)$ may be specified as follows:

$$H_{X_b}(\omega)=\frac{N_{X_b}(\omega)}{D_{X_b}(\omega)};\ H_Y(\omega)=\frac{N_Y(\omega)}{D_Y(\omega)}$$

where $D_Y(\omega)=D_{X_b}(\omega)$ and

$$\begin{gathered}N_{X_b}(\omega)=-\mathbf{r}^{\mathbf{T}}\mathbf{M}_s\mathbf{d}(\omega)\mathbf{M}_s\mathbf{r}\alpha^2\omega^6\mu_l+M_{tot}\alpha^2\omega^4\mu_l\\(\beta+\mu_t-1)+\\+b(\omega)c(\omega)M_{tot}(1+\mu_t)(\beta+\mu_t)+\omega^2(\beta+\\+\mu_t)(c(\omega)M_{tot}\mu_t+\ +b(\omega)c(\omega)\mathbf{r}^{\mathbf{T}}\mathbf{M}_s\mathbf{d}(\omega)\mathbf{M}_s\mathbf{r}+\\+b(\omega)M_{tot}\alpha^2\mu_l;\\D_{X_b}(\omega)=-\mathbf{r}^{\mathbf{T}}\mathbf{M}_s\mathbf{d}(\omega)\mathbf{M}_s\mathbf{r}\alpha^2\omega^8\mu_l-a(\omega)b(\omega)c(\omega)\\M_{tot}(\beta+\\+\mu_t)+2M_{tot}\alpha^2\omega^6\mu_l(\beta+\mu_t)+\omega^4\left(b(\omega)\left(M_{tot}\alpha^2\mu_l+\right.\right.\\\left.+c(\omega)\mathbf{r}^{\mathbf{T}}\mathbf{M}_s\mathbf{d}(\omega)\mathbf{M}_s\mathbf{r}\right)(\beta+\mu_t)+M_{tot}\left(a(\omega)\alpha^2\mu_l+\\\left.+c(\omega)(\beta+\mu_t)^2\right)\end{gathered}$$

$$\begin{gathered}N_Y(\omega)=a(\omega)c(\omega)M_{tot}\mu_t+M_{tot}\omega^2\left(a(\omega)\alpha^2\mu_l+c(\omega)\right.\\(1+\mu_t)(\beta+\\\left.+\mu_t)\right)+\omega^4\left(c(\omega)\mathbf{r}^{\mathbf{T}}\mathbf{M}_s\mathbf{d}(\omega)\mathbf{M}_s\mathbf{r}\beta+\ M_{tot}\alpha^2\mu_l\right.\\\left.(1+\beta+\mu_t)\right)\end{gathered}$$

Moreover,

$$\begin{aligned}H_U(\omega)&=\frac{\alpha}{c(\omega)}\left[-1+\omega^2H_{\mathbf{X}_s}(\omega)+\omega^2H_Y(\omega)\right];\ H_{\mathbf{Xs}}(\omega)\\&=\mathbf{d}(\omega)\left(\omega^2\mathbf{M}_s\mathbf{r}H_{X_b}(\omega)-\mathbf{M}_s\mathbf{r}\right)\end{aligned}\tag{A.3}$$

Once these functions have been evaluated, the response variances in terms of container displacement, liquid displacement, and main structure displacements can be determined numerically by solving the following equations:

$$\sigma_Y^2=\int_0^\infty|H_Y(\omega)|^2G_0\,d\omega$$

$$\sigma_U^2=\int_0^\infty|H_U(\omega)|^2G_0\,d\omega\tag{A.4}$$

$$\sigma_{\mathbf{Xs}}^2=\int_0^\infty|H_{\mathbf{Xs}}(\omega)|^2G_0\,d\omega$$

APPENDIX B

In this appendix, the procedure for a more rigorous estimation of the head loss coefficient is outlined. The base displacement variance of the BI subsystem subjected to a white noise process can be obtained by using the following

integral form reported by Roberts and Spanos (1990)

$$\sigma_{X_b}^2 = \frac{G_0}{2}\int_0^\infty \frac{\Xi_m(\omega)}{\Lambda_m(-i\omega)\Lambda_m(i\omega)}d\omega \tag{A.5}$$

where

$$\begin{aligned}\Xi_m(\omega) &= \vartheta_{m-1}\omega^{2m-2} + \vartheta_{m-2}\omega^{2m-4} + \cdots + \vartheta_0;\\ \Lambda_m(i\omega) &= \lambda_m(i\omega)^m + \lambda_{m-1}(i\omega)^{m-1} + \cdots + \lambda_0;\end{aligned} \tag{A.6}$$

Specifically, the variance of $\sigma_{X_b}^2$ in Equation (A.5) (for $m = 6$) can be expressed as

$$\sigma_{X_b}^2 = \frac{\begin{vmatrix} \vartheta_5 & \vartheta_4 & \vartheta_3 & \vartheta_2 & \vartheta_1 & \vartheta_0\\ -\lambda_6 & \lambda_4 & -\lambda_2 & \lambda_0 & 0 & 0\\ 0 & -\lambda_5 & \lambda_3 & -\lambda_1 & 0 & 0\\ 0 & \lambda_6 & -\lambda_4 & \lambda_2 & -\lambda_0 & 0\\ 0 & 0 & \lambda_5 & -\lambda_3 & \lambda_1 & 0\\ 0 & 0 & -\lambda_6 & \lambda_4 & -\lambda_2 & \lambda_0 \end{vmatrix}}{\begin{vmatrix} \lambda_5 & -\lambda_3 & \lambda_1 & 0 & 0 & 0\\ -\lambda_6 & \lambda_4 & -\lambda_2 & \lambda_0 & 0 & 0\\ 0 & -\lambda_5 & \lambda_3 & -\lambda_1 & 0 & 0\\ 0 & \lambda_6 & -\lambda_4 & \lambda_2 & -\lambda_0 & 0\\ 0 & 0 & \lambda_5 & -\lambda_3 & \lambda_1 & 0\\ 0 & 0 & -\lambda_6 & \lambda_4 & -\lambda_2 & \lambda_0 \end{vmatrix}} \frac{\pi G_0}{2\lambda_6} \tag{A.7}$$

where $\lambda_i (i = 0, .., 6)$ and $\vartheta_j (j = 0, \dots, 5)$ are constant coefficients and the vertical lines || mean the determinant of the matrix. The definition of $\lambda_i (i = 0, .., 6)$ and $\vartheta_j (j = 0, \dots, 5)$ is presented below:

$$\begin{aligned}
&\lambda_6 = \beta - \alpha^2\mu_l + \mu_t;\\
&\lambda_5 = 2\omega_b(\beta+\mu_t)\left[\zeta_2\left(1+\beta-\alpha^2\mu_l+\mu_t\right)\nu_2 + \zeta_l\nu_l\right];\\
&\lambda_4 = \omega_b^2\left[-\alpha^2\mu_l\left(1+(\beta+\mu_t)\nu_2^2\right) + (\beta+\mu_t)\left(1+(1+\beta+\mu_t)\nu_2^2 + \right.\right.\\
&\left.\left. + 4\zeta_2\zeta_l(1+\beta+\mu_t)\nu_2\nu_l + \nu_l^2\right]\right];\\
&\lambda_3 = 2\omega_b^3(\beta+\mu_t)\left[\zeta_l\left(1+(1+\beta+\mu_t)\nu_2^2\right)\nu_l + \right.\\
&\left. + \zeta_2\nu_2\left(1+(1+\beta+\mu_t)\nu_l^2\right)\right];\\
&\lambda_2 = \omega_b^4(\beta+\mu_t)\left[4\zeta_2\zeta_l\nu_2\nu_l + \nu_l^2 + \nu_2^2\left(1+(1+\beta+\mu_t)\nu_l^2\right)\right];\\
&\lambda_1 = 2\omega_b^5\nu_2\nu_l(\beta+\mu_t)(\zeta_l\nu_2 + \zeta_2\nu_l); \lambda_0 = \omega_b^6\nu_2^2\nu_l^2(\beta+\mu_t);
\end{aligned} \tag{A.8}$$

$$\begin{aligned}
&\vartheta_5 = 0; \vartheta_4 = \left(\beta - \alpha^2\mu_l + \mu_t\right)^2;\\
&\vartheta_3 = 2(\beta+\mu_t)\left[\left(\alpha^2\mu_l - \mu_t - 1\right)\left(\beta - \alpha^2\mu_l + \mu_t + \right.\right.\\
&\left. + 2\zeta_2^2\left(\alpha^2\mu_l - \mu_t - 1\right)(\beta+\mu_t)\nu_2^2 - 4\alpha^2(\beta-1)\zeta_2\zeta_l\mu_l\nu_2\nu_l + \right.\\
&\left.\left. + \left(\alpha^2\mu_l - \beta - \mu_t + 2\zeta_l^2(\beta+\mu_t)\right)\nu_l^2\right]\omega_b^2;\right.\\
&\vartheta_2 = (\beta+\mu_t)\left[(\beta+\mu_t)\left(1-\alpha^2\mu_l+\mu_t\right)^2\nu_2^4 + \right.\\
&+ 2\left(-\alpha^2(1+\beta)\mu_l + 2\left(\beta - \alpha^2\mu_l\right)\mu_t + 2\mu_t^2 + \right.\\
&+2(\beta+\mu_t) - 4\zeta_l^2(1+\mu_t)(\beta+\mu_t) + \\
&\left.\left. +4\zeta_2^2(1+\mu_t)(\beta+\mu_t)\left(\alpha^2\mu_l - 1 - \mu_t + 2\zeta_l^2(1+\mu_t)\right)\right)\nu_2^2\nu_l^2 \right.\\
&\left. + \ +(\beta+\mu_t)\nu_l^4\right]\omega_b^4;\\
&\vartheta_1 = 2(1+\mu_t)(\beta+\mu_t)^2\nu_2^2\nu_l^2\left[\left(\alpha^2\mu_l - 1 - \mu_t + 2\zeta_l^2(1+\mu_t)\right)\right.\\
&\left.\nu_2^2 + \ +\left(-1+2\zeta_2^2(1+\mu_t)\right)\nu_l^2\right]\omega_b^6;\\
&\vartheta_0 = (1+\mu_t)^2(\beta+\mu_t)^2\nu_2^4\nu_l^4\omega_b^8;
\end{aligned} \tag{A.9}$$

It is worth noting that the expressions in Equations (A.8) and (A.9) and thus the variance in (A.7) include the equivalent damping ratio ζ_l, compared to the variance computed by means of Equation (11) where it was neglected. By numerically minimizing the variance in (A.7) and considering the input structural parameters obtained by means of the proposed procedure, the optimal value of the equivalent damping ratio ζ_l can be obtained.

As previously stated, the formulation presented in this appendix has been derived considering a white noise base excitation. However, in the case of more generic broadband earthquake excitation, such as the Kanai–Tajimi stationary filtered white noise process, previously introduced in Section 4, the same integral formulation can be adopted. Specifically, since this kind of filter, characterized by the one-sided PSD reported in Equation (19), adds two degrees of freedom to the original system, the numerator and denominator of the expression in Equation (A.7) would imply matrices with dimensions 8×8 and $\lambda_i (i = 0, .., 8)$ and $\vartheta_j (j = 0, \dots, 7)$, thus leading to rather complex formulae of λ_i and ϑ_j here not reported for the sake of brevity. Moreover, considering that, as shown in Section 4, the proposed approach, based on the white noise assumption, practically matches the numerical solution even when implementing a Kanai–Tajimi filter, on the light of the great computational gain achieved, the proposed formulae can be considered as accurate enough for the purpose of the present optimization problem.